Engineering Structures 308 (2024) 117937

Contents lists available at ScienceDirect

Engineering Structures

journal homepage: www.elsevier.com/locate/engstruct

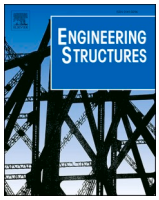

Seismic design spectra considering nonlinear connections between the existing building and the retrofit system

Simone Labò *, Andrea Belleri, Alessandra Marini

University of Bergamo, Department of Engineering and Applied Sciences, Italy

ARTICLE INFO

Keywords:
Exoskeleton
Retrofit
Design spectra
Connections
Preliminary design

ABSTRACT

Holistic retrofit solutions for RC buildings carried out from the outside through structural exoskeletons, have been widely proposed in recent years. Based on the need to further investigate this type of intervention, the interaction between the existing building and the external exoskeleton was studied and discussed using a simplified 2DOF model. Both elastic and nonlinear retrofit solutions were considered. In the nonlinear case, the nonlinearity of the retrofit was lumped into the connection between the elements representing the existing building and the exoskeleton, yet the simplified model could be slightly adjusted to account for the nonlinearity in all its elements. The main contribution of the paper is the definition of design spectra aimed at the preliminary proportioning of elastic and nonlinear seismic retrofit solutions. Based on existing building characteristics, the developed design spectra provide the minimum retrofit stiffness required to achieve a given target displacement and, in the case of a nonlinear retrofit, the connection stiffness and yielding force that minimizes such displacement. The proposed design spectra allow for a direct comparison of the response of different retrofit solutions thus defining the optimal parameters for the retrofit system; the advantages and disadvantages of introducing elastic and nonlinear retrofit solutions may be discussed. A simplified design method was proposed and validated through nonlinear analyses applied to a 3D case study resembling an existing RC building that requires seismic retrofit. The case study validates the design spectra findings highlighting how the use of nonlinear connection could minimize the displacement. Furthermore, it highlights the beneficial effects of nonlinear connections in reducing the burden on the foundation of the new retrofit system and in reducing the seismic actions in the existing floors.

1. Introduction

The pursuit of a safe and sustainable society requires the renovation of the existing building stock, which is obsolescent and inherently vulnerable to natural hazards such as earthquakes [3]. To address this issue, interest in integrated retrofit solutions carried out from the outside of the building has increased in recent years. The potential of this approach has been recognized as it allows the integration of energy, structural, and architectural interventions, reduces intervention times and costs by performing multiple interventions simultaneously, and overcomes one of the main obstacles to renovation, namely occupant relocation and building disruption [14,21,25,28,29,37,4,48,6]. Suitable retrofit solutions for this approach include diagonal exoskeletons [11,12,17,23,8,9,31,30,41], and the shell solution of Marini and Zanni [51,52], Smiroldo et al., [45], Santansiero et al. [43], Sancin et al. [42], Manfredi et al. [27], Passoni et al. [36], Zanni et al. [53].

Although some technological applications have already been proposed, the study of the structural behavior of such retrofit systems still deserves attention, and the problem of proposing simple methods for the preliminary design of elastic and nonlinear retrofit solutions needs further study. Ciampi et al. [5] addressed the problem by describing the behavior of the retrofitted system through a simplified single-degree of freedom (DOF) model. After introducing a single DOF to represent a building equipped with dissipative bracing, the behavior of the entire system was evaluated through parametric analyses and nonlinear design response spectra were derived. Feroldi [14] proposed a simplified model to evaluate the behavior of retrofit solutions. Nonlinear time history analyses were performed on simplified finite element models with only one DOF to understand the behavior of the retrofitted system and derive design criteria for elastic and nonlinear retrofit exoskeletons.

In recent years, new simplified models and approaches have further explored the behavior of these solutions. Labò et al. [24] have developed a new approach and numerical method based on a 2DOF system: starting

* Corresponding author.
E-mail address: simone.labo@unibg.it (S. Labò).

https://doi.org/10.1016/j.engstruct.2024.117937
Received 21 November 2023; Received in revised form 7 March 2024; Accepted 24 March 2024
Available online 11 April 2024

Nomenclature

2DOF symbols

$\widetilde{k}$	Equivalent stiffness of the retrofit (connection+exoskeleton)
$\widetilde{c}$	Equivalent damping of the retrofit (connection+exoskeleton)
$\widehat{k}$	Total stiffness of the SDOF system
$\widehat{V}$	Total soliciting action of the SDOF system
V_1	Soliciting action of the *element 1*
$\widetilde{V}$	Soliciting action of the equivalent spring
$\widetilde{\lambda}$	Stiffness ratio: $\widetilde{k}/\ k_1$
c_1	Damping coefficient of the *element 1*
c_{12}	Damping coefficient of the connection
c_2	Damping coefficient of the *element 2*
$F_{y,1}$	Yielding force of the bi-linear curve of the *element 1*
$F_{y,12}$	Yielding force of the bi-linear curve of the connection
k_1	Initial elastic stiffness of the *element 1*
k_{12}	Initial elastic stiffness of the connection
k_2	Initial elastic stiffness of the *element 2*
m	Mass of the equivalent SDOF system
m_1	Effective mass of the *element 1*
m_2	Effective mass of the *element 2*
$S_a(T)$	Design spectrum acceleration
$S_d(T)$	Design spectrum displacement
u_1	Displacement of the *element 1*
u_2	Displacement of the *element 2*
u_{12}	Relative displacement between the two *elements* (u_2-u_1)
$u_{1,MAX}(i_\delta, i_{GM})$	Maximum displacement experienced by the *element 1* when subjected to the GM (i_{GM}) and when the yielding displacement $\delta_{y,12}(i_\delta)$ is considered
$F_{12}(u_{1,MAX})$	Force in the connection when $u_1(i_\delta, i_{GM}) = u_{1,MAX}(i_\delta, i_{GM})$
$u_{1,AVG}(i_\delta, i_\mu)$	The average values of the maximum displacement experienced by the *element 1* when subjected to a set of GMs
$F_{12,AVG}(i_\delta, i_\mu)$	The average force in the connection when $u_1(i_\delta, i_\mu) = u_{1,AVG}(i_\delta, i_\mu)$
$u_{1,MIN}(i_\mu)$	Minimum value of the average values of the maximum displacement experienced by the *element 1* when subjected to a set of GMs
$F_{12}(u_{1,MIN})$	Force in the connection when $u_{1,AVG}(:, i_\mu) = u_{1,MIN}(i_\mu)$
$\ddot{X}_g$	Ground acceleration
$\delta_{y,1}$	Yielding displacement of the bi-linear curve of the *element 1*
$\delta_{y,12}$	Yielding displacement of the bi-linear curve of the connection
δ_{MAX}	Target maximum displacement for the *element 1*
η	Yield force adimensionalized with respect to the mass (m_1) multiplied by the ground acceleration ($Sa(T_1)$)
T_1	Elastic period of the element 1; $T_1 = 2\pi\sqrt{\frac{m_1}{k_1}}$
λ	Stiffness ratio:k_2/k_1
μ	Ductility demand
μ_{NL}	Ductility demand when *NL* connection are considered
μ_{ROI}	Range of interest of μ
$\delta_{y,12\text{-}ROI}$	Range of interest of $\delta_{y,12}$
i_μ	Index of the range of interest of μ
i_δ	Index of the range of interest of $\delta_{y,12}$
i_{GM}	Index of the considered ground motion
β	Yielding displacement ratio ($\delta_{y,12}/\delta_{y,1}$)
ζ	Yielding force ratio ($F_{y,12}/F_{y,1}$)
$\overline{\zeta}$	Optimal yielding force ratio ($F_{y,12}/F_{y,1}$)
θ	Inter-story drift ratio target
$P(t)$	Nonlinear force introduced according with the Bouc Wen model
Z	Internal variable of the Bouc Wen model
α	Post yielding stiffness ratio
n	Dimensionless quantity that governs the smoothness of the nonlinear behavior in the proximity of the yielding point
ν	Dimensionless quantity that controls the size of the nonlinear hysteretic loop
γ	Dimensionless quantity that controls the shape of the nonlinear hysteretic loop

MDOF symbols

d_{TOP}	Target maximum top displacement of the existing building
d	Top displacement of the existing building
Δ	Top drift of the existing building
d_i	Interstory displacement of the existing building
Δ_i	Interstory drift of the existing building
σ_s	Soil stress (0.3 MPa)
k_s	Unit soil stiffness
Γ	Participation factor
m_i	Mass of the -*i* floor
ϕ_i^1	Eigenvector of the 1st mode in the AS-IS condition
d_i^1	Eigenvector of the 1st mode in the retrofitted condition
k_{i-12}^{EL}	Elastic stiffness of the elastic connections at the -*i* floor
k_{i-12}^{NL}	Elastic stiffness of the nonlinear connections at the -*i* floor
F_{i-12}^{NL}	Yielding force of the nonlinear connections at the -*i* floor
$k_{i,f}$	Equivalent lateral stiffness of the existing building in the AS-IS condition
$k_{i,eq}$	Equivalent lateral stiffness of the retrofit at the -*i* floor (connection+exoskeleton)

from the preliminary considerations in Feroldi [14] and Ciampi et al. [5], the authors proposed design spectra for the preliminary design of elastic retrofit solutions. In Faiella et al. [12], the behavior of the retrofitted system was studied using modal and linear dynamic spectral analyses by varying the parameters describing the simplified model (2 DOF system), focusing on diagonal exoskeletons. In Reggio et al. [41], the response of a simplified, rigidly coupled, 2 DOF system to a basic harmonic excitation was analyzed as a function of system parameters. The influence of the connection between the two DOFs was preliminarily analyzed by Labò [22] considering both elastic and nonlinear connections in parametric analyses of a 2 DOF system. The present work builds on these contributions by defining a simplified strategy for deriving preliminary design parameters for elastic and nonlinear retrofits, especially in the case of nonlinear connections.

The existing building and exoskeleton are described by the equations of motion of a 2 DOF system, and the preliminary design parameters are represented by a compact graphical design tool (design spectra) that combines the idealized nonlinear response of the retrofitted building with the elastic and nonlinear properties of the retrofit system. The proposed design spectra allow a direct comparison of the response of different retrofit solutions thus defining the optimal parameters for the retrofit system. In this work, the nonlinearity of the retrofit lies in the connections between the exoskeleton and the existing building, although the approach can be easily extended to account for the

nonlinearity of the exoskeleton itself. The proposed method, although derived for externally performed retrofit solutions, can be easily extended to other retrofit solutions (e.g., endoskeletons) and applications (e.g., it could be integrated into loss assessment analyses).

Section 2 presents the simplified 2 DOF model, key assumptions, and parameters used to describe the existing building and the retrofit exoskeleton. Section 3 presents preliminary and necessary considerations for the simplified model based on the results of previous works [12,22,24,41]. The main novelty of the paper lies in Section 4 in which the method and the processes of deriving design spectra for elastic and nonlinear retrofit solutions are described, and some example of design spectra and their possible use are presented. In Section 5, a new design procedure based on the use of design spectra is proposed and applied to a reference case study resembling an existing RC building not designed for seismic actions.

2. Development of a simplified 2 DOF model

The interaction between the existing building (hereafter *element 1*) and the retrofit solution (hereafter *element 2*) is described by a 2 DOF system consisting of 2 masses connected by springs (k_1, k_2, k_{12}) and viscous dampers (c_1, c_2, c_{12}), and subjected to a ground acceleration ($\ddot{X}_g$). Fig. 1 shows the considered 2 DOF system.

Element 1 is defined by the effective mass (m_1), the elastic stiffness (k_1), the damping coefficient (c_1), and the yielding force ($F_{y,1}$); for a given elastic stiffness and yielding force, the yielding displacement ($\delta_{y,1}$) is known ($\delta_{y,1} = F_{y,1}/k_1$). *Element 2* is assumed to be elastic, and it is defined by the elastic stiffness (k_2) and the damping coefficient (c_2). The two masses are connected by a general link described by its elastic stiffness (k_{12}) and damping coefficient (c_{12}). In the case of nonlinear connection (*NL*), the connection yielding force ($F_{y,12}$) and the corresponding yielding displacement ($\delta_{y,12}$) are introduced (Fig. 1b).

The structural response is analyzed with reference to a set of basic parameters identified following the literature review (Eq. 1), where β and ζ refer only to the nonlinear case.

$$\eta = \frac{F_{y,1}}{[m_1 \cdot S_a(T_1)]} \quad \mu = \frac{\delta_{MAX}}{\delta_{y,1}} \quad \lambda = \frac{k_2}{k_1} \quad \beta = \frac{\delta_{y,12}}{\delta_{y,1}} \quad \zeta = \frac{F_{y,12}}{F_{y,1}} \tag{1}$$

- η is the dimensionless yielding strength of the existing building, obtained by dividing the yielding strength by the product of the building mass (m_1) and the spectral acceleration at the elastic period of *element 1*, $S_a(T_1)$.
- μ is the ductility parameter expressed as the ratio between the maximum displacement (δ_{MAX}) experienced by the retrofitted *element 1* during a seismic event and the yielding displacement of *element 1* ($\delta_{y,1}$).
- λ is the ratio between the elastic stiffness of the retrofit (k_2) and the stiffness of the existing building (k_1).
- β is the ratio between the yielding displacement of the connection in the *NL* case ($\delta_{y,12}$) and the yielding displacement of *element 1* ($\delta_{y,1}$).
- ζ is the ratio between the yielding force of the connection in the *NL* case ($F_{y,12}$) and the yielding force of *element 1* ($F_{y,1}$).

2.1. Equations of motion and solving method

For each mass, Newton's second law of motion yields:

$$\begin{cases} \boldsymbol{m_1}\left(\ddot{\boldsymbol{X}}_g + \ddot{\boldsymbol{u}}_1\right) + \boldsymbol{k_1 u_1} + \boldsymbol{c_1 \dot{u}_1} = \boldsymbol{k_{12}}(\boldsymbol{u_2} - \boldsymbol{u_1}) + \boldsymbol{c_{12}}(\dot{\boldsymbol{u}}_2 - \dot{\boldsymbol{u}}_1) \\ \boldsymbol{m_2}\left(\ddot{\boldsymbol{X}}_g + \ddot{\boldsymbol{u}}_2\right) + \boldsymbol{k_2 u_2} + \boldsymbol{c_2 \dot{u}_2} = -\boldsymbol{k_{12}}(\boldsymbol{u_2} - \boldsymbol{u_1}) - \boldsymbol{c_{12}}(\dot{\boldsymbol{u}}_2 - \dot{\boldsymbol{u}}_1) \end{cases} \tag{2}$$

The nonlinear behavior of *element 1* and, in the *NL* case, of the connection is modeled by the Bouc-Wen hysteresis law reported in Eqs. 3 and 4 [50]. The nonlinear behavior of *element 1* and the connection is accounted for by replacing $k_1 u_1$ and $k_{12}(u_2 - u_1)$ in Eq. 2 with *P(t)* (Eq. 3) where the subscript *-i* is set equal to 1 for *element 1* and equal to 12 for the connection; the displacement u_{12} refers to the relative displacement between the two *elements* (u_2-u_1).[1]

$$\boldsymbol{P}(\boldsymbol{t}) = \boldsymbol{\alpha} \cdot \boldsymbol{k_i} \cdot \boldsymbol{u_i} + (\boldsymbol{1} - \boldsymbol{\alpha}) \boldsymbol{k_i} \cdot \boldsymbol{\delta_{y,i}} \cdot \boldsymbol{Z}(\boldsymbol{t}) \tag{3}$$

where α is the post-yielding stiffness ratio (supposed equal to 1/1000 in all cases), and Z is an internal variable whose behavior is described by its derivative:

$$\frac{\boldsymbol{dZ}}{\boldsymbol{dt}} = \left(\frac{\boldsymbol{1}}{\boldsymbol{\delta_{y,i}}}\right) \cdot \left(\dot{\boldsymbol{u}}_i - \boldsymbol{\gamma} \cdot |\dot{\boldsymbol{u}}_i| \cdot \boldsymbol{Z}(\boldsymbol{t}) \cdot |\boldsymbol{z}(\boldsymbol{t})|^{\boldsymbol{n-1}} - \boldsymbol{\upsilon} \cdot \dot{\boldsymbol{u}}_i \cdot |\boldsymbol{z}(\boldsymbol{t})|^{\boldsymbol{n}}\right) \tag{4}$$

n, ν, and γ are dimensionless quantities assumed herein equal to 1, 0.5, and 0.5, respectively. n determines the smoothness of the curve near the yield point, ν and γ control the size and shape of the hysteretic loop ($|\nu|+|\gamma|=1$).

The equations of motion (Eq. 2) are solved using the Ode45 function (MathWorks, 2017), a versatile solver for ordinary differential equations that applies the Runge-Kutta method with a variable time step. The algorithm requires the transformation of the second-order differential equations into an equivalent system of first-order equations.

2.2. Input parameters

The input parameters were chosen to be representative of ordinary European post-WWII buildings as highlighted by Marini et al. [29]. As for the yielding force, different values of η were considered ($\eta = 0.30$, 0.50–0.60, 0.85), according with Ciampi, et al., [5]. Since low to mid-rise buildings were considered (ranging from 3 to 7 floors), the fundamental period of the existing building has been taken in the range of 0.8 s-1.2 s according to $T_1 = 0.071 \cdot H^{0.96}$, where H is the height of the building expressed in meters [49]. The range takes into account a reduced elastic modulus in RC elements to consider cracked sections. Regarding the retrofit solution for RC buildings, the mass of *element 2* (m_2) was assumed to be 1/10 - 1/20 of the mass of *element 1* [25,51].

For the ground acceleration ($\ddot{X}_g$), seven accelerograms[2] compatible with the Life Safety Limit State (LSLS) code spectrum were obtained from [19]. A maximum scale factor of 2 and upper and lower tolerances of 10% and 15% were specified for the ground motion selection. The building is supposed located in L'Aquila (Italy) on a flat surface with soil category C and topography T1 [35]. Because the design spectra are expressed in terms of the strength parameter (η), the influence of the site seismicity on the results is not considered herein.

3. Preliminary considerations on elastic and nonlinear connections

Preliminary considerations based on the results of previous research are presented in this section for both elastic (*EL*) and nonlinear (*NL*) retrofit solutions (i.e., elastic, and nonlinear connection). These considerations form the basis for the proposed method (Section 4).

[1] By substituting (3) in (2)

$$\begin{cases} m_1\left(\ddot{X}_g + \ddot{u}_1\right) + (\alpha \cdot k_1 \cdot u_1 + (1-\alpha) k_1 \cdot \delta_{y,1} \cdot Z(t)) + c_1 \dot{u}_1 \\ \qquad = (\alpha \cdot k_{12} \cdot u_{12} + (1-\alpha) k_{12} \cdot \delta_{y,12} \cdot Z(t)) + c_{12}(\dot{u}_2 - \dot{u}_1) \\ m_2\left(\ddot{X}_g + \ddot{u}_2\right) + k_2 u_2 + c_2 \dot{u}_2 = -(\alpha \cdot k_{12} \cdot u_{12} + (1-\alpha) k_{12} \cdot \delta_{y,12} \cdot Z(t)) - c_{12}(\dot{u}_2 - \dot{u}_1) \end{cases}$$

[2] Record code [1] and scale factor in brackets: 001726ya (1.11), 000133xa (2.76), 000600xa (1.75), 000335ya (2.50), 001726xa (1.36), 000879ya (0.94), 000592ya (1.51).

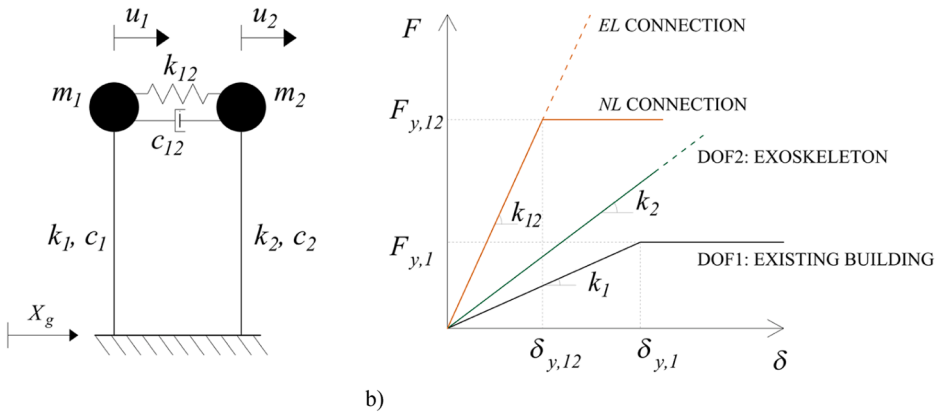

Fig. 1. a) simplified 2 DOF model; b) response curves of each component of the 2 degrees of freedom (2 DOF) working in parallel; *EL* and *NL* refer to the elastic and nonlinear cases, respectively.

3.1. Elastic connection

If the connection between the two elements is elastic and the fundamental mass of the exoskeleton (m_2) is small compared to the fundamental mass of the existing building (m_1), the elastic system can be simplified to a single DOF system with equivalent mass (m) equal to the sum of m_1 and m_2 (being m_2 small compared to m_1, its contribution can be neglected or assumed to be equal to 1/10–1/20 m_1). *Element 2* and the connection are considered as 2 springs connected in series (Fig. 2a) and can be lumped together (Fig. 2b) [12,24,41]. Among others, Labò et al. [24] demonstrated such an assumption by analyzing the frequency response of *element 1* due to a unit force in *element 1* through the 2 DOF system transfer matrix and showed that when the m_2/m_1 mass ratio is less than 1/10, the whole system can be described by considering only one mode of vibration (the one with the lowest frequency). The same consideration was made when k_2 was significantly higher than k_1 (k_2/k_1 higher than 8 – see Appendix 1). The transfer matrix ($T(\omega)$) of the system and some considerations are reported in Appendix 1.

By modeling the connection and exoskeleton (*element 2*) as two springs in series, k_{12} and k_2 respectively, the equivalent stiffness and damping of the retrofit can be represented as in Eq. 5a and Eq. 5b, and the equivalent stiffness ratio is redefined as given in Eq. 5c.

$$\widetilde{k} = \frac{k_2 k_{12}}{k_2 + k_{12}} \tag{5a}$$

$$\widetilde{c} = \frac{c_2 c_{12}}{c_2 + c_{12}} \tag{5b}$$

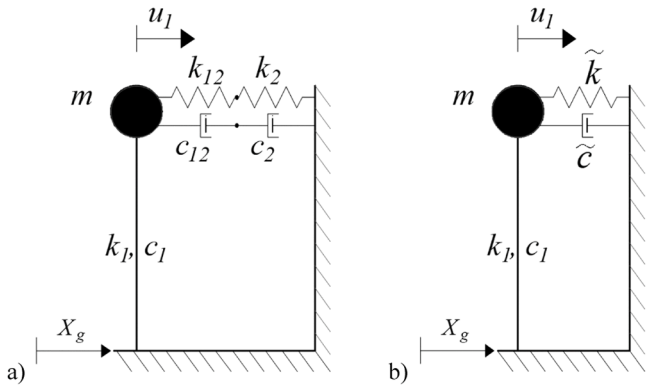

Fig. 2. a) simplified SDOF system; b) simplified SDOF system with equivalent spring and damping.

$$\widetilde{\lambda} = \frac{\widetilde{k}}{k_1} \tag{5c}$$

3.2. Nonlinear connection

In the case of nonlinear connection, the best performance, resulting in the minimum required ductility demand on the existing building, is found by plotting μ as a function of the connection yielding displacement ($\delta_{y,12}$) or connection yielding force ($F_{y,12}$). Since for a reference case $\delta_{y,1}$ and $F_{y,1}$ are constants, the same consideration can be made by plotting μ as a function of $\beta = \frac{\delta_{y,12}}{\delta_{y,1}}$ or $\zeta = \frac{F_{y,12}}{F_{y,1}}$ (Fig. 3). Therefore, $\delta_{y,12}$ or $F_{y,12}$ (i.e., β or ζ in Fig. 3) in correspondence to the minimum μ represents the optimal connection design.

Fig. 3 shows the ductility demand (μ) as a function of the yielding displacement ratio (β) (Fig. 3a and d) and force ratio (ζ) (Fig. 3b and e). In Fig. 3a and b η varies from 0.3 to 0.85, while in Fig. 3d and e, for a given η, different values of $\widetilde{\lambda}$ were considered, representing retrofits with low, medium, and high stiffness ratios; $\widetilde{\lambda}$ equal to 0.5 leads to the results of the AS-IS condition ($\widetilde{\lambda} = 0$), while $\widetilde{\lambda}$ equal to 6.7 can be considered a reasonable upper limit for equivalent retrofit stiffness since no significant benefits were observed by introducing a retrofit solution with higher stiffness [14]. In the manuscript, AS-IS refers to the unretrofitted condition. When $\widetilde{\lambda}$ is varied, only the stiffness of the connection changes. Fig. 3c and f show qualitatively how the parameters are varied.

Fig. 3a, and b show that for the same value of connection yielding force and displacement, respectively, the higher η is, the lower is μ. This is reasonable considering that buildings with higher η are expected to experience lower displacement than buildings with lower η when retrofitted with the same retrofit solution. The higher the value of β (and hence of ζ), the closer the ductility demand μ approaches the elastic response, e.g., for β greater than 0.4, the connections can be considered elastic. However, the most important consideration is that all curves have a minimum stationary point, therefore, for certain values of β (or ζ), the displacement demand of the existing building (*element 1*) can be minimized ($u_{1,MIN}$). The connections should be designed according to these values. The optimal yield point of the connection shifts significantly to the left by increasing η: the smaller the strength parameter (η) is, the higher the yield value of the connection should be (i.e., the higher the shear force on the exoskeleton).

Additional considerations are reported in the following (each one refers to the minimum point indicated by its respective number in Fig. 3d and e):

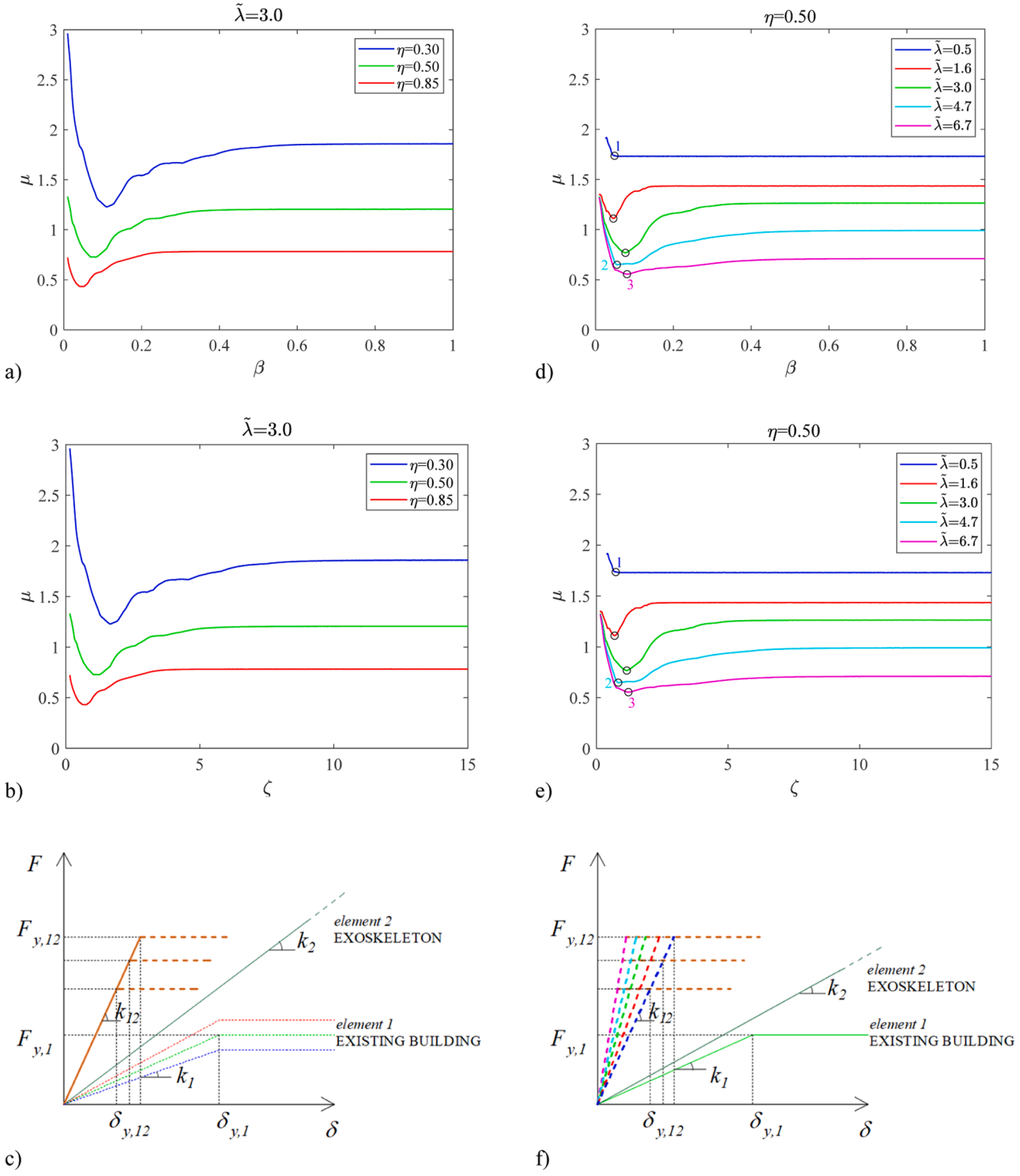

Fig. 3. Ductility demand (μ) on the existing building (*element 1*) as a function of the yielding displacement ratio (β), and the yielding force ratio (ζ). In (a) and (b) the value of $\tilde{\lambda}$ is set and the parameter η is varied while in (d) and (e) η is set and $\tilde{\lambda}$ is varied. In (c) and (f) the varied parameters are qualitatively represented.

1) A unique stationary point is not always present (point 1 in Fig. 3d and e): for low values of λ, the elastic solution represents the optimal solution with respect to the displacement requirement of *element 1*.
2) In some cases, the numerical minimum point is at the side of a minimum region (the locus of points in which μ is minimized). In such cases, as point 2 in Fig. 3d and e, a lower value of the connection yielding would entail a significant increase in terms of μ. Therefore, a more central optimal yield value in the minimum region should be selected.
3) For a high value of λ (point 3 in Fig. 3d and e) the *NL* solution does not entail significant improvements compared to an elastic solution (high value of ζ).

4. Design spectra

This section describes the method used to generate elastic and nonlinear design spectra; elastic (*EL*) and nonlinear (*NL*) refers to the behavior of the connection between *element 1* and *element 2,* which was alternatively considered elastic and nonlinear. Starting from the parameters used to describe *element 1* (m_1, k_1, c_1, $\delta_{y,1}$), design spectra are defined by performing sensitivity analyses for varying properties of the simplified systems (single DOF and 2 DOFs systems for elastic and nonlinear design spectra, respectively); the ductility demand of the existing building (μ) and the optimal yielding force of the connection (ζ) are plotted as a function of the equivalent stiffness ratio ($\tilde{\lambda}$).

The entire process is described in Fig. 4. The subsection of the flowchart related to elastic spectra (*EL*) ends with the "*NL analyses*" selection operator (Fig. 4); accordingly, the sub-cycle contained in the

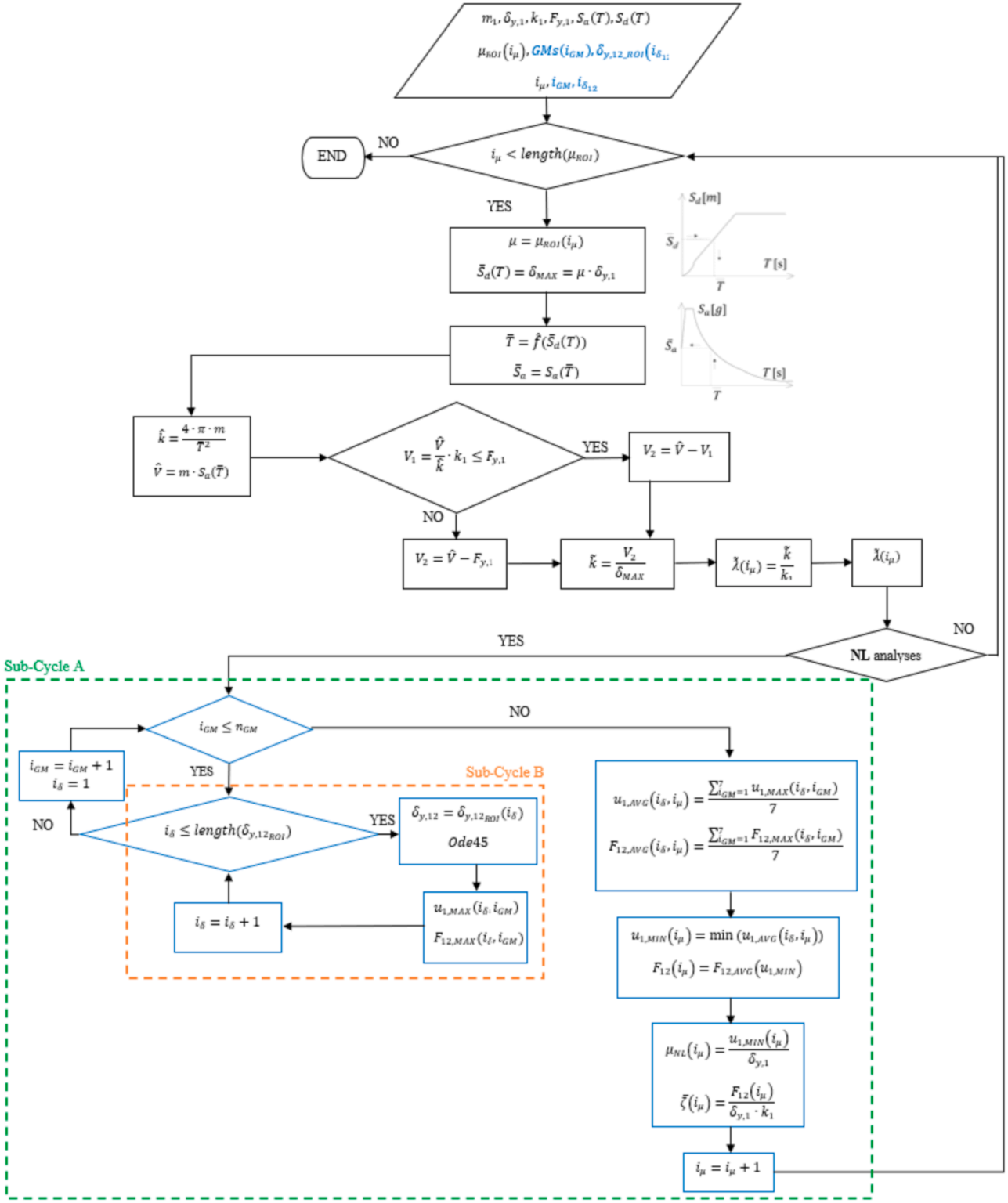

Fig. 4. Flow chart for elastic and nonlinear design spectra.

dotted green box – Sub-Cycle A – refers to the nonlinear design spectra (*NL*). In Fig. 4, the input parameters and the edge of the boxes that refer to the *NL* case are colored blue. New arrays must be introduced to define the parameter range of interest (denoted by the subscript *ROI* in Fig. 4) in which the sensitivity analyses are performed; these are μ_{ROI} (range in which μ is varied) and $\delta_{y,12\text{-}ROI}$ (range in which $\delta_{y,12}$ is varied), and for both an index -*i* have been introduced to indicate the position within the array itself (i_μ and i_δ, respectively). In the *NL* case, the equations of motion are solved for various ground motions (*GMs*) identified with the index i_{GM}.

4.1. Elastic design spectra

A cycle of the process related to the derivation of elastic spectra is described herein. All the considerations are based on the single DOF system shown in Fig. 2. Given *element 1* parameters (m, k_1, c_1, $\delta_{y,1}$), and site spectra ($S_a(T)$,$S_d(T)$), the spectral displacement ($\overline{S}_d$) for $\mu = \mu_{ROI}(i_\mu)$ can be identified as $\overline{S}_d = \mu \bullet \delta_{y,1} = \delta_{MAX}$. Once the displacement spectrum is defined, the elastic period ($\overline{T}$) and the pseudo acceleration ($S_a(\overline{T})$) can be derived from the displacement and acceleration spectrum (Fig. 4). Consequently, the total elastic stiffness ($\widehat{k}$) and the total load demand ($\widehat{V}$) on the system can be calculated as

$$\widehat{k} = \frac{4 \bullet \pi^2 \bullet m}{\overline{T}^2} \qquad \widehat{V} = m \bullet S_a(\overline{T}) \tag{6}$$

Defining V_1 as the load on *element 1* corresponding to its initial stiffness (k_1) and its maximum capacity ($F_{y,1}$) (Eq. 7a), the load demand on the two springs in series ($\widetilde{V}$) can be calculated as shown in Eq. 7. Recall that with two springs in series $\widetilde{V}$ is equal to V_2.

$$\begin{cases} \text{if} \quad V_1 = \dfrac{\widehat{V}}{\widehat{k}} \bullet k_1 \le F_{y,1} \longrightarrow \widetilde{V} = \widehat{V} - V_1 \\ \text{if} \quad V_1 = \dfrac{\widehat{V}}{\widehat{k}} \bullet k_1 > F_{y,1} \longrightarrow \widetilde{V} = \widehat{V} - F_{y,1} \end{cases} \tag{7}$$

Consequently, the equivalent stiffness ($\widetilde{k}$) can be calculated as

$$\widetilde{k} = \frac{\widetilde{V}}{\delta_{MAX}}, \widetilde{\lambda}(i_\mu) = \frac{\widetilde{k}}{k_1} \tag{8}$$

Elastic spectra are then obtained by varying the input parameter μ within the range of interest (μ_{ROI}) and different curves can be derived by varying *element 1* parameters. For example, design spectra for different elastic periods (T_1) are found by varying the effective mass (m_1) (i.e., by varying the equivalent mass m) or the elastic stiffness (k_1); otherwise, the design spectra for $\eta = 0.30$, 0.50–0.60, and 0.85 are obtained by varying the strength parameter (η) (i.e., by varying the input parameter $F_{y,1}$).

4.2. Nonlinear design spectra

The nonlinear spectra are derived in Sub-cycle A (Fig. 4), which is implemented for each iteration of the elastic process (i.e., for each $\mu = \mu_{ROI}(i_\mu)$ and, consequently, for each $\widetilde{\lambda}(\mu(i_\mu))$. By solving the nonlinear equations of motion for a selected set of ground motions, the objective of sub-cycle A is to identify the yielding force of the connection ($F_{y,12}$) that minimizes the ductility demand (μ_{NL}), i.e., identify the minimum point of the $\mu(\delta_{y,12})$ curve (e.g., those shown in Fig. 3) for each loop of the *EL* process.

Let's consider the 2 DOFs system of Fig. 1: the equations of motion (Eq. 2) are solved using the Ode45 function [47] for each of the selected ground motions (*GM* (i_{GM})) by varying the yielding displacement of the connection ($\delta_{y,12}(i_\delta)$) within the range of interest ($\delta_{y,12\text{-}ROI}(i_\delta)$), i.e. Sub-cycle B in Fig. 4; then the maximum displacement ($u_{1,MAX}(i_\delta, i_{GM})$) and the corresponding connection force $\left(F_{12}\left(u_{1,MAX}\right)\right)$ are derived. When all ground motions have been processed (herein when $i_{GM} > n_{GM}$), the average values of the maximum displacement ($u_{1,AVG}(i_\delta, i_\mu)$) and average force ($F_{12,AVG}(i_\delta, i_\mu)$) are calculated for each value of the connection yielding displacement ($\delta_{y,12}(i_\delta)$).

A similar trend to the one plotted in Fig. 3 would be obtained by calculating $u_{1,AVG}(i_\delta, i_\mu)$ for all μ values in the *ROI* and plotting $\mu(i_\delta, :) = \frac{u_{1,AVG}(i_\delta,:)}{\delta_{y,1}}$ as a function of β or ζ. At this point, among all cases in $\delta_{y,12\text{-}ROI}$, the minimum value of the average maximum displacement can be found ($u_{1,MIN}(i_\mu)$) for each *NL* loop and the corresponding force in the connection can be determined ($F_{12}(i_\mu) = F_{12,AVG}(u_{1,MIN})$). Thus, the new ductility demand corresponding to the *NL* model ($\mu_{NL}(i_\mu)$) and the normalized optimal yielding force of the connection ($\overline{\zeta}(i_\mu)$) can be derived:

$$\mu_{NL}(i_\mu) = \frac{u_{1,MIN}(i_\mu)}{\delta_{y,1}} \overline{\zeta}(i_\mu) = \frac{F_{12}(i_\mu)}{\delta_{y,1} \bullet k_1} \tag{9}$$

An example of design spectra is plotted and described in the following.

4.3. General considerations and sensitivity analysis

Some general considerations and a sensitivity analysis are reported herein. For this purpose, the equivalent spring is referred to as the "*retrofit solution*", because it represents both the connection and the exoskeleton for a retrofit system, and *element 1* is the "*existing building*". The range of interest (*ROI*) in which the parametric analysis was performed is shown in Table 1. $\mu_{ROI}(i_\mu)$ was chosen to be representative of an ordinary post-WWII RC building; $\widetilde{\lambda} = 0$ represents the AS-IS condition and $\widetilde{\lambda} = 7$ is a reasonable upper value for the equivalent retrofit stiffness [14]. $\delta_{y,12\text{-}ROI}(i_\delta)$ ranges in the interval [0 - $\delta_{y,1}$], thus setting as the upper bound the condition in which the connection yields when the existing building yields [22]. The seven ground motions presented in Section 2.2 were considered.

Fig. 5 shows the design spectra for a given value of the existing building period in the AS-IS condition (T_1=1.00 s) and a given value of the strength parameter ($\eta = 0.50$). The graph shows the ductility demand (μ) for the *EL* and *NL* cases (in a black and grey solid line, respectively); being μ expressed as the ratio between the maximum displacement (δ_{MAX}) experienced by the retrofitted *element 1* during a seismic event and the yielding displacement of *element 1* ($\delta_{y,1}$), even if an elastic retrofit solution is added (*EL*), *the element 1* (i.e., *the existing building)* may experience a displacement higher than $\delta_{y,1}$; in these cases, the ductility parameter μ can be higher than 1.

As for the nonlinear case (*NL*) the optimal yield ratio ($\overline{\zeta}$) (with blank circles) for the *NL* case as a function of the equivalent stiffness ratio ($\widetilde{\lambda}$). The blank circles refer to the exact minimum point found by applying the numerical procedure described in Section 4. Based on the considerations of Section 3 (Fig. 3d and e):

1) μ_{NL} is not drawn unless a significant reduction in displacement was found: a displacement reduction greater than 5% of the *EL* case was considered.
2) A minimum region (Fig. 3b, and e) was defined considering the range of ζ associated with μ values at most 5% higher than the $\min\left(\mu\left(\widetilde{\lambda}\right)\right)$,

Table 1
Range of parameters used in the sensitivity analysis.

Parameter	Symbol	Interval
Ductility demand	$\mu_{ROI}(i_\mu)$	[$\mu(\widetilde{\lambda}$=0) - $\mu(\widetilde{\lambda}$=7)]
Connection yielding displacement	$\delta_{y,12\text{-}ROI}(i_\delta)$	[0 - $\delta_{y,1}$]

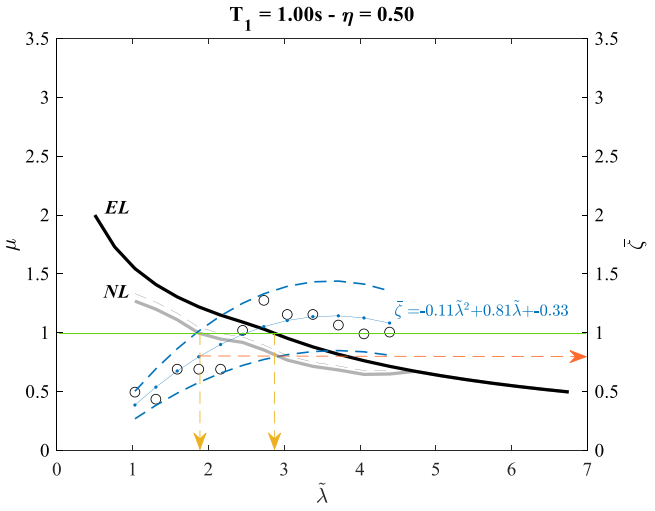

Fig. 5. Example of *EL* spectrum (black line) and *NL* spectrum (grey line); empty circles indicate the optimal values of the yielding forces ($\bar{\zeta}$) as a function of the equivalent stiffness ($\tilde{\lambda}$). The trend line of the minimum points (empty circles) is plotted in blue); the trend lines of the minimum region edges are plotted with blue dashed lines.

i.e. the minimum point found numerically by the procedure in Section 4.

The trend line of the minimum points is plotted in blue (Fig. 5), while the trend lines of the minimum region edges are plotted with blue dashed lines. It is worth noting that the maximum increase in μ_{NL} that can occur by choosing values in the minimum region is about 10% and is shown in Fig. 5 with a dashed gray line.

As expected, the response of the system depends on the stiffness of the retrofit solution. For both *EL* and *NL*, $\tilde{\lambda} = 0$ represents the AS-IS condition associated with the maximum damage. As the stiffness of the retrofit increases, the ductility demand decreases. Fig. 5 shows that in the *EL* case, high benefits in terms of ductility demand can be obtained by increasing $\tilde{\lambda}$ up to $\tilde{\lambda} = 3$, i.e., the value beyond which the system behaves elastically. However, to further reduce the ductility demand of the existing building beyond certain limits, very stiff (and possibly over-resistant) solutions are required. As for the nonlinear case, Fig. 5 shows that by introducing a nonlinear connection, the ductility demand decreases more compared to the *EL* case; for $\tilde{\lambda} < 1$, no unique minimum point could be identified, while the ductility demand of the *NL* case is equal to that of the *EL* case for $\tilde{\lambda} > 4.5$. In general, the introduction of a nonlinear connection decreases the required equivalent stiffness ($\tilde{\lambda}$); for example, for $\mu = 1$, the minimum stiffness decreases from about $\tilde{\lambda} = 3$ to about $\tilde{\lambda} = 2$.

4.3.1. Use of the design spectra

Once the parameters of the existing building are defined (T_1, m_1, k_1, η) and the target ductility demand μ of *element 1* is determined (e.g., as a function of the maximum allowable drift of the existing structure), the stiffness of the retrofit can be derived by multiplying the stiffness ratio ($\tilde{\lambda}$) obtained from the spectra and the stiffness of the existing building (k_1). Both the elastic and the nonlinear retrofit stiffnesses can be derived in this way. Moreover, in the *NL* case, the optimal yield force ($\bar{\zeta}$) of the connection can be derived by the trend line equation by introducing the value of $\tilde{\lambda}$ obtained from the spectra for the *NL* case. Given $\bar{\zeta}$, the optimal yielding force of the connection can be derived as $F_{y,12} = \bar{\zeta} \bullet F_{y,1}$. To give an example, with T_1= 1.00 s and $\eta = 0.50$ (Fig. 5), to obtain a ductility μ equal to 1, $\tilde{\lambda}$ equal to 2.9 and 1.9 are required for the elastic and nonlinear cases, respectively. In the case of a nonlinear connection, the optimal value of $\bar{\zeta}$ is given by $\bar{\zeta} = -0.11\tilde{\lambda}^2 + 0.81\tilde{\lambda} - 0.33$ where $\tilde{\lambda}$ is set equal to 1.9. Given $\bar{\zeta}$, the optimal yielding force of the connection can be derived as $F_{y,12} = \bar{\zeta} \bullet F_{y,1}$.

Fig. 6 shows the *EL* and *NL* spectra for different values of η and T_1. The nonlinear curves were plotted until a minimum point could be identified.

As expected, μ decreases with increasing $\tilde{\lambda}$ in all cases, and the slopes of the curves are higher for low values of $\tilde{\lambda}$ while the slopes reduce when increasing $\tilde{\lambda}$. If an elastic retrofit is introduced in an existing building with T_1= 1 and $\eta = 0.50$, the value of μ decreases from 2 to 1 as $\tilde{\lambda}$ increases from 0.5 to 3, while it only decreases by 0.5 when $\tilde{\lambda}$ is increased from 3 to 7. When η is equal to 0.30, the slope decreases even more while increasing $\tilde{\lambda}$. Moving from $\tilde{\lambda}$ equal to 1 to $\tilde{\lambda}$ equal to 3.5, the value of μ reduces from 3 to 1.5. By increasing the stiffness of the retrofit up to 7 times the stiffness of the existing building, the value of μ reduces to 0.75.

For a fixed μ, the required retrofit stiffness ($\tilde{\lambda}$) increases as the capacity of the existing building (η) decreases, while the damage increases in the case of η equal to 0.30 for a fixed $\tilde{\lambda}$. In T_1= 1, an elastic solution provides a μ value of 1 when $\tilde{\lambda}$ is around 0.5 and η is 0.85, whereas a $\tilde{\lambda}$ value of approximately 5 is required when η is 0.30 to give the same μ ($\mu = 1$). Conversely, when $\tilde{\lambda}$ is equal to 1, the μ value increases from 0.9 to 3 for η values of 0.85 and 0.30, respectively.

Increasing T_1 provides a flattening of the spectra and the range where nonlinearities provide benefits increases. For the *NL* case, the lower the value of η (i.e., the lower the load-carrying capacity of the structure), the higher the required yielding force of the connection. In T_1= 1 and $\tilde{\lambda}$ equal to 3, $\bar{\zeta}$ moves from about 0.6 to about 1.9, for $\eta = 0.85$ and $\eta = 0.30$, respectively. It is worth noting that the range of $\tilde{\lambda}$ where nonlinearities are effective is significantly reduced for $\eta = 0.30$; in this case, the introduction of nonlinear retrofits must be carefully considered.

4.3.2. Considerations on uncertainties

The structural assessment of existing buildings may be influenced by various uncertainties which may affect, for instance, the definition of the elastic period (T_1), the strength ratio (η), and the connection stiffness (k_{12}). To quantify the effects of uncertainties on the connection yielding parameters ($\delta_{y,12}$, $F_{y,12}$), sensitivity analyses were performed. The sensitivity analyses were performed by changing one parameter (P_i) at a time within a range of $\pm$ 0.30 P_i; the reference parameters were T_1= 1.00 s, $\eta = 0.50$, k_{12}= 444 kN/mm. Fig. 7 shows the maximum and minimum variability of $\delta_{y,12}$, $F_{y,12}$, β, and ζ as a function of T_1, η, k_{12} in terms of tornado diagrams. As per the definition of a tornado diagram, the parameters are arranged in order of importance, with the most influential parameter appearing at the top of the chart [38].

The optimal yielding displacement of the connection ($\delta_{y,12}$) is affected by 61% and 36% when the existing building period (T_1) and the connection stiffness (k_{12}) are varied, respectively. The maximum variability due to T_1 reduces up to 44% when the results are plotted in terms of β. The magnitude of the influence of k_{12} does not vary (36%).

The results are less scattered when the connection yielding parameter is expressed in terms of the yielding force ($F_{y,12}$ or, in the case of the normalized value, ζ); the influence of the parameter (k_{12}) (i.e., the influence of the resulting stiffness of the system made by the connection and the exoskeleton) is negligible (less than 5%). T_1 is the most affecting parameter. For the strength parameter, the variation is similar in all the cases (up to 20%).

From the result emerges that $\delta_{y,12}$, and β are more sensitive to the existing building uncertainties than $F_{y,12}$, and ζ which have shown a smaller range of variability; for this reason, design spectra were plotted as a function of ζ. Given the influence of the elastic period and the variability (30%) associated with the choice of the optimal connection yielding value, it is recommended that the design spectra are derived

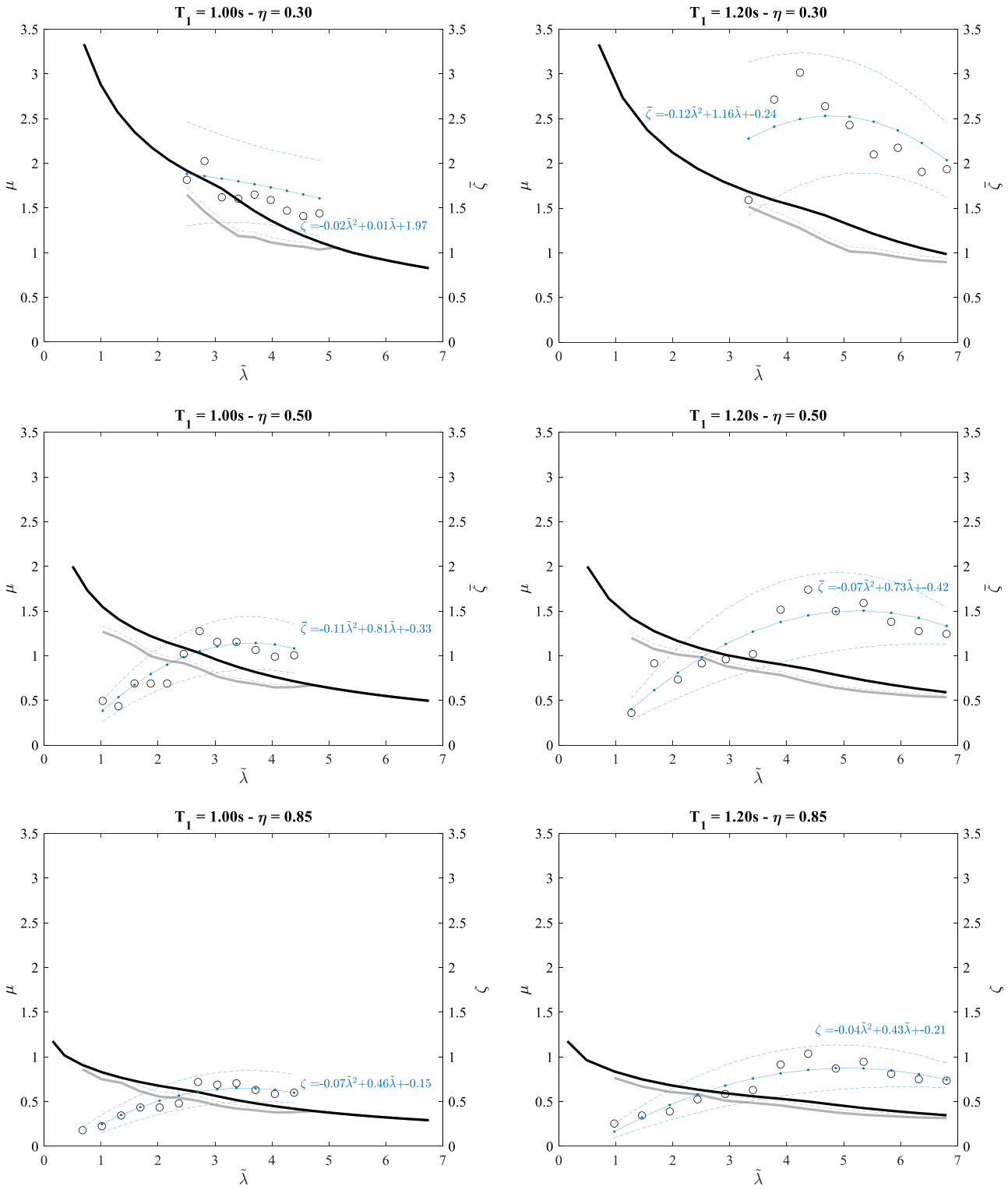

Fig. 6. Nonlinear design spectra for the preliminary design of retrofit solution from outside.

with a sufficiently narrow interval periods (steps of about 0.1 s).

It is worth remembering that the design would be finally validated by non-linear time history analyses.

5. Retrofit design procedure and validation

A preliminary design procedure is proposed and summarized in the following steps:

Step 1: Vulnerability analysis of the existing building and definition of the corresponding equivalent single DOF parameters.

Step 2: Definition of performance targets (e.g., maximum inter-story drift θ and top displacement d_{TOP}).

Step 3: Design of the retrofit solution: application of the design spectra to define the equivalent stiffness of the retrofit (exoskeleton and connections - $\tilde{k}$). Definition of the stiffness of the connection (k_{12}) and the exoskeleton (k_2), and, in the case of a nonlinear solution, the yielding

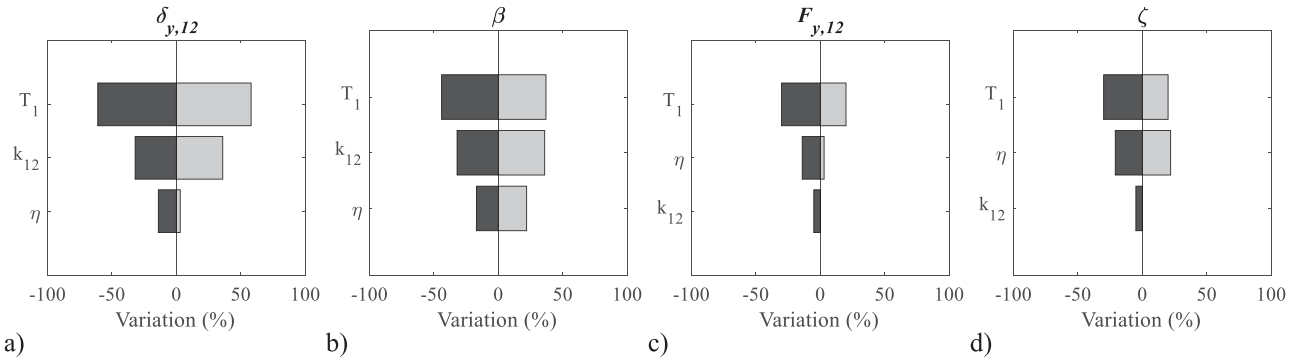

Fig. 7. Tornado plots representing the influence of the existing building parameters on the optimal connection yielding parameter: a) variation of the yielding displacement ($\delta_{y,12}$); b) variation of the normalized yielding displacement (β); c) variation of the yielding force ($F_{y,12}$); d) variation of the normalized yielding force (ζ).

force of the connections ($F_{y,12}$).

Step 4: SDOF to MDOF transformation according to [18] and [2].

Step 5: Validate the design through non-linear analyses (NLA).

5.1. Application to a case study

The selected case study is a residential four-story rectangular building (24.0 m x 10.6 m) with three one-way longitudinal frames and two infilled side frames. The inter-story height is 3.15 m. The structural system consists of RC frames in the longitudinal direction, designed to withstand gravity loads only. The main features and the structural details are reported in Appendix 2. The floors consist of a composite RC beam-and-clay-block system with a 4 cm thick RC overlay over a total thickness of 24 cm. The core of the staircase is not designed for seismic loads and consequently, the structural detailing did not allow for considering a global behavior among the three walls; three independent 20 cm thick walls were considered. The geometry of the main frame is shown in Fig. 8. An equivalent load of 1.20 kN/m^2 was considered to account for the partition walls while 2.00 kN/m^2 and 0.50 kN/m^2 were considered as live loads of internal floor (residential) and roof (not practicable), respectively [35].

A finite element model was developed using MidasGen [34]. Structural elements such as beams, columns, and the staircase core were modeled as beam elements with lumped plasticity in which shear and flexural behavior were modeled using European Building Code plastic hinges [10]. As for columns and staircase walls, the flexural yield strength is calculated considering the effect of axial force to reflect coupled axial force-biaxial moment behavior. The yield strength was automatically calculated based on the design code [10] and using the section information reported in Appendix 2.

The columns are assumed fixed at the base while a nonlinear rotational spring was introduced at the base of the staircase walls to simulate the stiffness of its footing and the associated flexural capacity of the soil. A unit soil stiffness (k_s) of 0.1 (N/mm^2)/mm and a maximum soil stress (σ_s) of 0.3 MPa were considered. The floors are modeled as in-plane rigid diaphragms. As for the nonstructural elements, existing masonry infills on the perimeter were modeled as two nonlinear compression-only equivalent trusses that converge at the beam-column joints. Cracking and peak forces were evaluated according to Decanini et al. [7], while the selected cracking and peak drifts were set at 0.3% for moderate damage and 0.5% for collapse, respectively [44]. A combination of in-plane and out-of-plane damage mechanisms was not addressed in this preliminary evaluation. It was assumed that setting a strict design target would help to control damages in non-structural components. However, in-plane and out-of-plane interaction of infill panels could be accounted for according to the available methods [32,33].

Nonlinear static analyses were performed to evaluate the structural performance of the reference building under the AS-IS conditions. Fig. 9a shows the capacity curve in the weakest direction of the building (*y*-direction in Fig. 8) and the associated damage; the base shear is plotted as a function of the top displacement (*d*) in the main *x*-axis and top inter-story drift (Δ) on the secondary *x*-axis. A lateral force distribution according to the first vibrational mode was considered [13]. In Fig. 9b,c the inter-story displacement and drift at Step 3 (plastic hinges at the base of the staircase walls and yielding of the columns at the base of Frame B), Step 9 (failure of the infill in Frame 1), Step 11 (failure of the first column at the base) are plotted, respectively.

Step 1: Vulnerability analysis of the existing building.

A vulnerability analysis is conducted according to the current Italian building code [35]. The reference building is supposed located in L'Aquila (soil category C and topography T1). The bi-linearized capacity

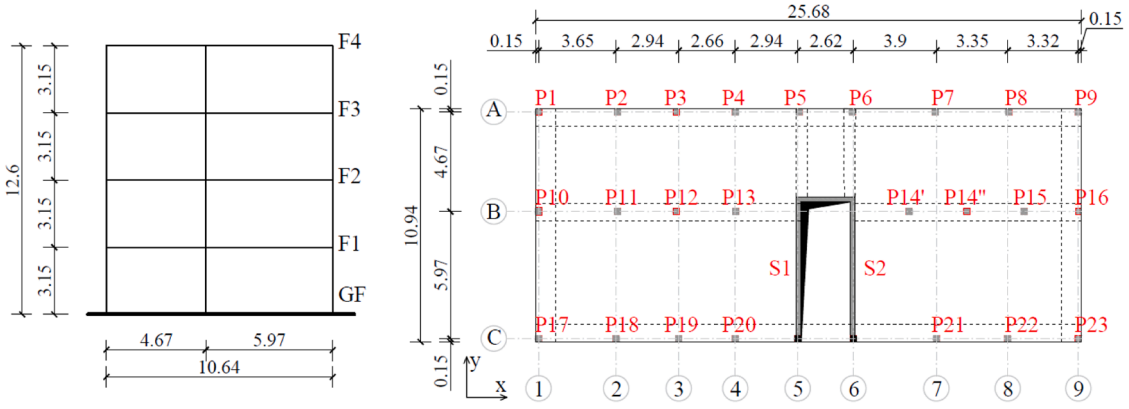

Fig. 8. Geometry of the reference building. Details in Appendix 2.

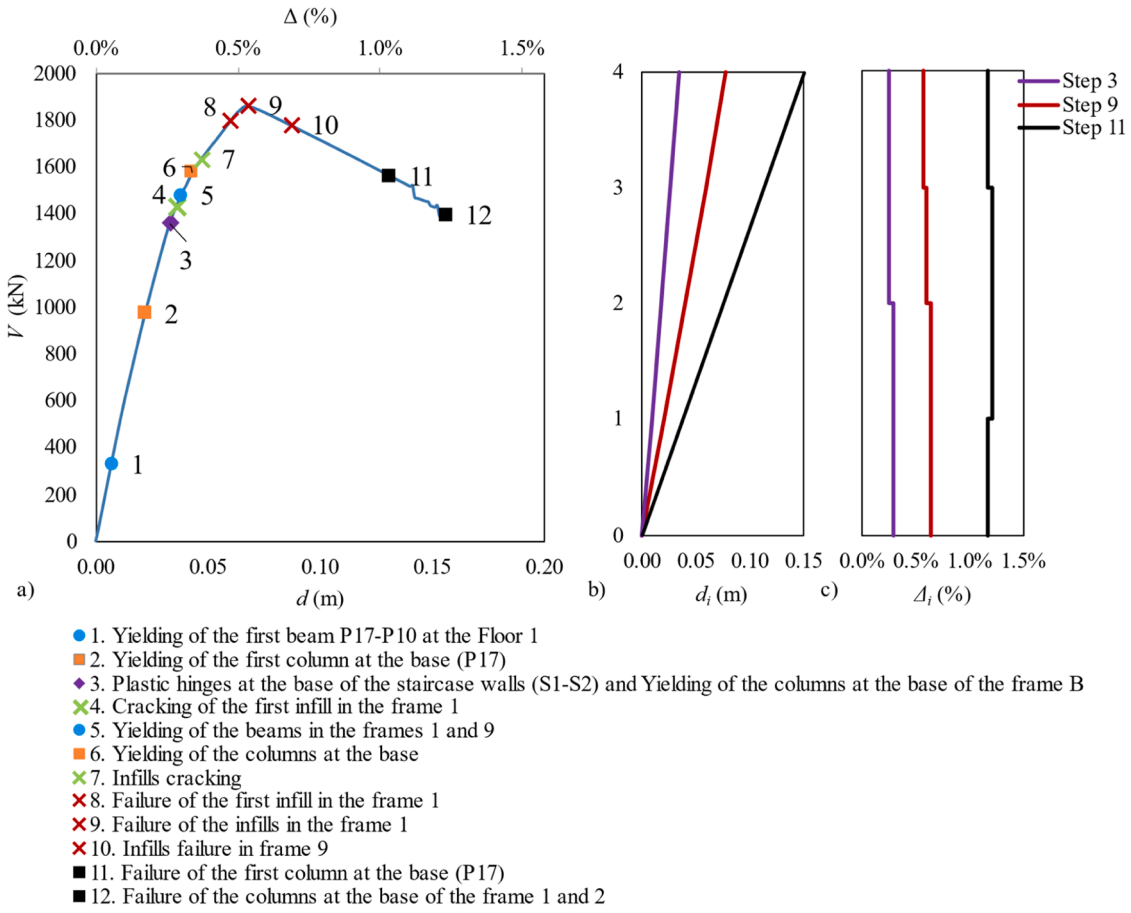

Fig. 9. a) capacity curve of the existing building; b) story displacement; c) inter-story drift. Note: The damage in (a) is indicated with dots for beams, squares for the columns, rhombuses for the staircase walls, and crosses for the infills.

curve and the displacement demands are plotted in ADRS terms in Fig. 10; the parameters of the equivalent SDOF system are given in Table 2. The collapse prevention limit state (*CPLS*) is set when one column first reaches its ultimate rotational capacity; the life safety limit state (*LSLS*) is set at ¾ of the rotation experienced at the *CPLS* [35].

As shown in Fig. 10, the existing building does not satisfy the displacement demands of the Life Safety Earthquake (*LSE*), return period equal to 475 years, and Collapse Prevention Earthquake (*CPE*), return period equal to 975 years, indicated with the vertical green and red dashed lines, respectively. Therefore, a structural retrofit is required.

Step 2: Definition of performance targets.

A maximum inter-story drift demand of 0.4% at the *LSE* is selected herein to avoid significant damage in the infills at this limit state (predicted at a drift of 0.5%). Assuming a seismic linear deformed shape of the retrofitted building, the correspondent top displacement allowable demand (d_{TOP}) is 0.05 m; by dividing the top displacement by the participation factor (Γ) the SDOF target displacement can be derived ($\delta_{MAX}=d_{TOP}/\Gamma$). The target ductility (μ) is the ratio between δ_{MAX} and the yielding displacement ($\delta_{y,1}$), which herein is 1.21.

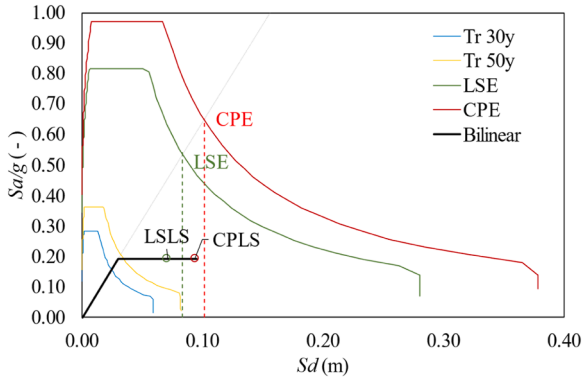

Fig. 10. Vulnerability analysis in the ADRS [35] for various limit states indicated with their return periods (*Tr*).

Table 2
Equivalent SDOF system parameters [35].

Equivalent SDOF	
m_1	632.1 kN/g
k_1	39.0 kN/mm
T_1	0.80 s
$F_{y,1}$	1196.1 kN
$\delta_{y,1}$	30.0 mm
Γ	1.39 (-)
η	0.37 (-)

Step 3: Definition of the parameters of the simplified 2DOF system.

Using the SDOF parameters of the existing building (Table 2) and the design spectra shown in Fig. 11, the retrofit parameters are derived. To guarantee the target μ value of 1.21, the required elastic stiffness of the retrofit ($\tilde{k}$) should be equal to 2.65 times the stiffness of the existing building (i.e. $\tilde{\lambda} = 2.65$); in the nonlinear case, the required $\tilde{\lambda}$ value is equal to 1.80 and the optimal connection yielding force ($F_{y,12}$) is equal to $0.82F_{y,1}$ (i.e., $\zeta(\tilde{\lambda})= 0.82$). It is worth noting that the SDOF parameters in Table 2 were derived through a nonlinear static procedure considering a lateral force distribution according to the first vibrational mode [13];

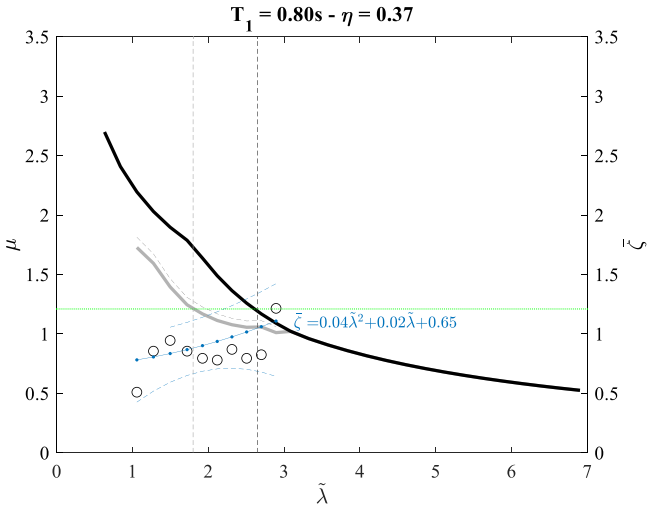

Fig. 11. Design spectra for the reference case. The green dotted line represents the target ductility. The grey and black dashed lines represent the minimum stiffnesses required for the *EL* and *NL* cases, respectively. In blue, the trend line of the optimal values of $\bar{\zeta}$.

the approach is therefore restricted to a single-mode response which is a valid hypothesis for low-rise buildings where the behavior is dominated by the fundamental vibration mode. However, the design procedure could be extended and used for other types of buildings such as tall buildings. For these structures, the conventional nonlinear static procedure may underestimate the seismic demand in the upper stories. In such cases, different pushover procedures can be investigated and implemented [46,39,20,40,16,26,15].

Step 4: SDOF to MDOF.

The properties of the MDOF system corresponding to the simplified system derived in Step 3 must be defined. In particular, the stiffness of both the connection and the exoskeleton, and in the *NL* case, the yielding force of the connection, must be derived for each floor of the existing building. For the sake of clarity, the floor parameters (i.e., the parameters of the MDOF system) are denoted by the subscript letter *i*. According to Guo & Christopolus (2013), the equivalent lateral stiffness of the existing building ($k_{i,f}$) is calculated as follows:

$$k_{i,f} = \left(\frac{2\pi}{T_1}\right)^2 \frac{\sum_{j=i}^{n} m_j \phi_j^1}{\Delta\phi_i^1} \boldsymbol{\Delta\phi_i^1 = \phi_i^1 - \phi_{i-1}^1; \Delta\phi_1^1 = \phi_1^1} \tag{10}$$

where the period of the existing building (T_1) and the mode shape $\{\phi_i^1\}$ are obtained from the eigenvalue analysis under the AS-IS condition. For the reference case T_1 is equal to 0.80 s and $\{\phi_i^1\}$ is given in Table 3.

According to Eq. 11, the equivalent stiffness (connection and exoskeleton) at each floor ($k_{i,eq}$) can be determined by imposing the mode shape $\{d_i^1\}$ of the retrofitted structure and by deriving the final period T_{FIN} of the retrofitted system (from the stiffness $\tilde{k}$ and the mass m). The mode shape $\{d_i^1\}$ may be different from the mode shape of the existing building (before the retrofit) since the introduction of the retrofit solution may force and regularize the fundamental mode shape. To give an example, a linear mode shape could be considered.

$$k_{i,eq} = \left(\frac{2\pi}{T_{FIN}}\right)^2 \frac{\sum_{j=i}^{n} m_j d_j^1}{\Delta d_i^1} - k_{i,f} \geq 0 \boldsymbol{\Delta d_i^1 = d_i^1 - d_{i-1}^1; \Delta d_1^1 = d_1^1} \tag{11}$$

For the reference case, the final period is equal to 0.42 s in the *EL* case and 0.49 s in the *NL* case.

As this work is a proof-of-concept, the stiffness of the connections (k_{i-12}) and the exoskeleton (k_{i-2}) are chosen without discussing their technical aspects. Since the reference case is regular in plan and elevation, the retrofit stiffness can be uniformly distributed along the building perimeter and, for simplicity, the same stiffness of the exoskeleton at each floor is considered (k_{i-2}), while the stiffness of the connections is calculated according to Eq. 5a (considering k_{i-2}, and $k_{i,eq}$ instead of k_2 and $\tilde{k}$). For the reference case, k_{i-2} is set equal to 555 kN/mm in the *EL* case and 612 kN/mm in the *NL* case. The stiffnesses of the connections at each floor are given in Table 3 as k_{i-12}^{EL} and k_{i-12}^{NL}, respectively.

Due to the in-plan and elevation regularity of the reference building, torsional and higher mode effects are not directly addressed in this preliminary evaluation, although their impact may be examined in future studies.

The yielding force on each floor is then derived according to Belleri [2]. More specifically, $F_{y,12}$ is distributed along the height of the building according to Eq. 12. The connection yielding force on each floor F_{i-12} is given in Table 3.

$$\boldsymbol{F_{i-12} = \frac{F_{y,12} m_i d_i^1}{\sum_{i=1}^{n} m_i d_i^1}} \tag{12}$$

It is worth noting that varying the connection yielding force along the building height may be difficult in practical terms or even impossible unless specific devices are used; such devices must be able to be calibrated in terms of stiffness and yielding force. To give an example, the Adesa fuses presented in [52] may be implemented. However, due to the significance of the technological aspects, they will be specifically addressed in future research.

Step 5: Design validation through NLA.

Nonlinear time history analyses were performed considering (a) the elastic retrofit solution (*EL*), where only the nonlinear behavior of the existing building is considered, and (b) the retrofit with dissipative connections (*NL*). The nonlinear connections are modeled by introducing hysteretic links between the existing building floors and the external exoskeleton: the same Bouc-Wen hysteretic model parameters used in the numerical model were considered. Since the technological aspects are not addressed in this work, the retrofit system is simply modeled by lumped masses (equal to 1/20 m_i) at each floor level interconnected by elastic links with stiffness k_{i-2}. Considering that the exoskeleton runs all around the perimeter of the building (i.e. 2 retrofit systems for each building principal direction), the values given in Table 3 must be divided by 2.

Seven ground motions compatible with the LSLS code spectrum were derived and applied in the y-direction of the reference building [19]. The average results of the 7 *GMs* refer to the *y*-direction and are summarized in Table 4 in terms of the maximum base shear of the whole system (V_{Max}), the maximum base shear of the retrofit (V'_{Max}), the maximum base shear of the existing building (V''_{Max}), and the maximum

Table 3
SDOF to MDOF procedure parameters.

Floor	m_i (kN/g)	ϕ_i^1	d_i^1	Elastic k_{i-2} (kN/mm)	Elastic k_{i-12}^{EL} (kN/mm)	Nonlinear k_{i-2} (kN/mm)	Nonlinear k_{i-12}^{NL} (kN/mm)	F_{i-12} (kN)
P4	199.7	1.00	1.00	555	165.2	612	92.2	307.3
P3	289.3	0.76	0.75		520.8		244.4	333.9
P2	289.3	0.51	0.50		1055.6		379.0	222.6
P1	290.6	0.26	0.25		1616.3		462.6	111.8

Table 4
Time history average results.

		V_{Max} (kN)	V'_{Max} (kN)	V''_{Max} (kN)	d_{TOP} (m)	ϑ_{TOP} (%)
EL	*Avg*	8690	2084	6591	0.050	0.40
	S.D.	2797	734	1216	0.017	0.13
NL	*Avg*	4753	1451	3271	0.046	0.39
	S.D.	902	407	301	0.006	0.06

floor displacement and inter-story drift (d_{TOP}, ϑ_{TOP}). Fig. 12 shows the time history results of the elastic (*EL*) and the non-linear (*NL*) solutions, expressed in terms of floor acceleration, inter-story drift, and lateral displacement of the top floor.

For both the elastic (*EL*) and the nonlinear (*NL*) cases, a good agreement is observed between the target top floor drift (ϑ_{TOP}=0.4%) and the results of the analyses (average drift values obtained from the 7 GMs), demonstrating the effectiveness of the proposed design procedure; moreover, the inter-story drift does not exceed the target drift value in either case. A 47% reduction in the total base shear (V_{Max}) is shown when nonlinear connections are introduced between the existing building and the exoskeleton (*NL*); also, the acceleration of the top floor decreases from 0.83 g to 0.44 g. These aspects become relevant when designing the foundation of the retrofit system or when the seismic forces in the existing floors need to be limited. Moreover, the results of the *NL* case are less scattered than those of the elastic retrofit solution (*EL*).

6. Major research contributions

This work is part of ongoing research aimed at fostering the holistic renovation of existing RC buildings not designed for seismic actions and requiring deep renovation. The paper contributes to the research through the definition of new design spectra particularly suitable for the preliminary design of elastic and nonlinear retrofit solutions carried out from the outside.

The spectra were derived by solving the equations of motion of a simplified 2 degrees of freedom system representative of an existing

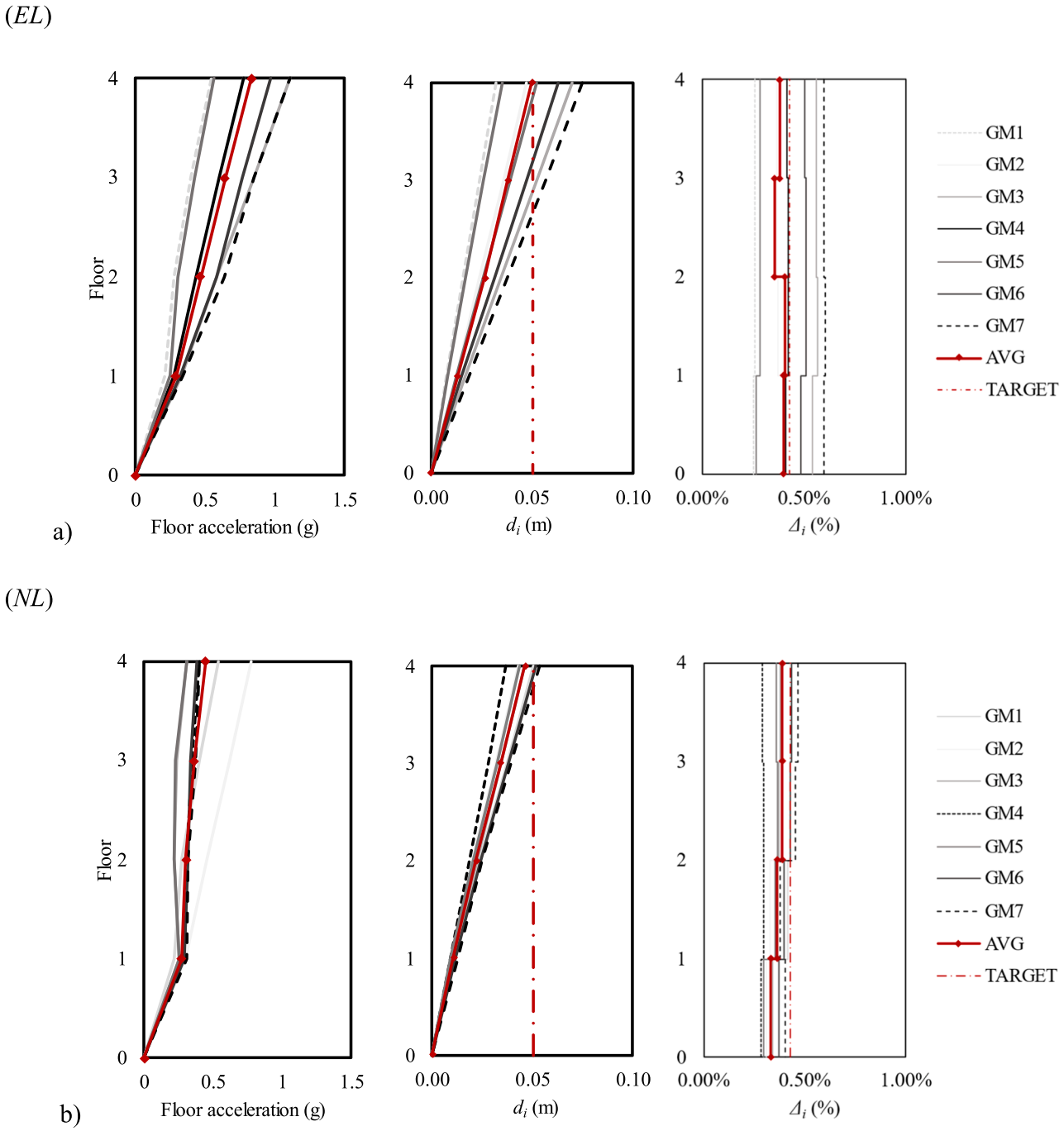

Fig. 12. Floor acceleration, story displacement, and inter-story drift: a) in case of elastic connections (*EL*); b) in case of non-linear connections (*NL*).

building and the associated retrofit system (e.g., a possible exoskeleton). The two elements are connected by either elastic or nonlinear connections. The nonlinearity of the exoskeleton could also be considered by applying the same model.

These spectra are tools that allow deriving the optimal mechanical characteristics of the retrofit solution, such as the minimum required elastic stiffness and the optimal yield strength of the nonlinear connection which minimize the displacement experienced by a retrofitted building.

They allow for a direct comparison of the response of different retrofit solutions thus defining, for example, the most cost-effective solution or the optimal parameters for a retrofit solution.

It is important to specify that while the system used to obtain the spectra is simple, it also has its own limitations and boundaries. It is important to understand the limitations and hypotheses on which design spectra are built to best utilize them; the above considerations can be applied in a broader sense when the structural behavior of a retrofitted building can be described using a 2DOF system and can be characterized by a fundamental vibration mode.

Moreover, design spectra must be used aware of the existing building uncertainties. Uncertainties are connected to the existing materials and the structural detailing, to modeling issues such as the nonlinear behavior of the infill panels and the staircase core, among others. The study found that creating design spectra based on the connection yielding force helps to minimize the impact of existing building parameters (and consequently, their uncertainties) but a successful design carefully also considers these aspects.

By giving it due attention, design spectra may be useful for researchers, to develop statistical or parametric analyses, or to be integrated into loss-cost analyses, innovative multicriteria assessments, or innovative design frameworks, and for practitioners, as they could be used, for example, for the preliminary design of the retrofit solutions and the comparisons between different retrofit strategies. Design spectra may be the starting point for a mindful design of a retrofit solution which accounts for the conceptual design and the technological and architectural aspects.

To give an example of design spectra application, a procedure for the design of seismic retrofit solutions such as exoskeletons was proposed considering the derived design spectra. Since design spectra were derived based on a 2DOF system, the method has been validated by nonlinear time history analyses on a 3D reference existing RC building. A regular building was considered; the impact of torsional and higher mode effects is postponed to specific and future studies.

From the results emerged how the use of nonlinear connections could be beneficial in reducing the burden on the foundation of the new retrofit system and in reducing the seismic actions in the existing floors.

CRediT authorship contribution statement

Alessandra Marini: Writing – review & editing, Supervision, Methodology, Conceptualization. **Andrea Belleri:** Writing – review & editing, Visualization, Supervision, Methodology, Conceptualization. **Simone Labò:** Writing – original draft, Visualization, Methodology, Investigation, Data curation, Conceptualization.

Declaration of Competing Interest

The authors declare that they have no known competing financial interests or personal relationships that could have appeared to influence the work reported in this paper.

Data availability

Data will be made available on request.

Acknowledgements

The authors greatly acknowledge the financial support of the University of Bergamo through the “STARS” research grant program and ReLuis which partially founded this work.

Appendix 1

Starting from the equations of motion (Eq. 2), the transfer matrix ($T(\omega)$) of the system described in Fig. 1 is derived. The solution of the equations of motion can be expressed as:

$$\begin{cases} \underline{u} = \underline{X}\cdot e^{i\omega\, t} \\ \dot{\underline{u}} = i\omega\, t\cdot\underline{X}\cdot e^{i\omega\, t} \\ \ddot{\underline{u}} = -\omega^2\cdot\underline{X}\cdot e^{i\omega\, t} \end{cases} \tag{A1}$$

By substituting (A1) in (Eq. 2), it yields:

$$\left[-\omega^2\underline{M} + i\omega\,\underline{C} + \underline{K}\right]\cdot\underline{X}\cdot e^{i\omega\, t} = \underline{F}\cdot e^{i\omega\, t} \tag{A2}$$

By defining the Impedance Matrix $Z(\omega)$ as:

$$\underline{Z}(\omega) = \left[-\omega^2\underline{M} + i\omega\,\underline{C} + \underline{K}\right] \tag{A3}$$

and, combining (A1) and (A2), it yields:

$$\underline{Z}(\omega)\cdot\underline{X} = \underline{F} \tag{A4}$$

The transfer matrix is the inverse of the impedance matrix $\underline{Z}(\omega)^{-1} = \underline{T}(\omega)$,

$$Z^{-1} = \frac{\begin{bmatrix} Z_{22} & -Z_{12} \\ Z_{21} & Z_{11} \end{bmatrix}}{\det|\underline{Z}|} = \begin{bmatrix} t_{11} & t_{12} \\ t_{21} & t_{22} \end{bmatrix}$$

where,

$$\det|\underline{Z}| = Z_{11}Z_{22} - {Z_{12}}^2 \tag{A5}$$

The solution can be expressed as:

$$\begin{Bmatrix} x_1 \\ x_2 \end{Bmatrix} = \begin{bmatrix} t_{11} & t_{12} \\ t_{21} & t_{22} \end{bmatrix} \begin{Bmatrix} F_1 \\ F_2 \end{Bmatrix} \tag{A6}$$

or in the compact form:

$$\underline{X} = [\underline{Z}(\omega)]^{-1}\underline{F} = \underline{T}(\omega)\cdot\underline{F} \tag{A7}$$

where $\underline{T(\omega)}$ is the transfer matrix and represents the behavior of the masses per unit input force as a function of the frequency.

By applying the described procedure to the reference system, the frequency response of the system when subjected to a harmonic load can be evaluated. The equations $T(i,j)$ of the transfer function that compose the transfer matrix $\underline{T(\omega)}$ of the 2 DOF system are:

$$T\left(1,1\right) = \frac{k_2 + k_{12} + i\cdot(c_2 + c_{12})\cdot\omega - m_2\cdot\omega^2}{-\left(-k_{12} - i\cdot c_{12}\cdot\omega\right)^2 + \left(k_1 + k_{12} + i\cdot\left(c_1 + c_{12}\right)\cdot\omega - m_1\omega^2\right)\cdot\left(k_2 + k_{12} + i\cdot\left(c_2 + c_{12}\right)\cdot\omega - m_2\omega^2\right)} \tag{A8}$$

$$T\left(1,2\right) = \frac{k_{12} + i\cdot c_{12}\cdot\omega}{-\left(-k_{12} - i\cdot c_{12}\cdot\omega\right)^2 + \left(k_1 + k_{12} + i\cdot\left(c_1 + c_{12}\right)\cdot\omega - m_1\omega^2\right)\cdot\left(k_2 + k_{12} + i\cdot\left(c_2 + c_{12}\right)\cdot\omega - m_2\omega^2\right)} \tag{A9}$$

$$T\left(2,1\right) = \frac{k_{12} + i\cdot c_{12}\cdot\omega}{-\left(-k_{12} - i\cdot c_{12}\cdot\omega\right)^2 + \left(k_1 + k_{12} + i\cdot\left(c_1 + c_{12}\right)\cdot\omega - m_1\omega^2\right)\cdot\left(k_2 + k_{12} + i\cdot\left(c_2 + c_{12}\right)\cdot\omega - m_2\omega^2\right)} \tag{A10}$$

$$T\left(2,2\right) = \frac{k_1 + k_{12} + i\cdot(c_1 + c_{12})\cdot\omega - m_1\cdot\omega^2}{-\left(-k_{12} - i\cdot c_{12}\cdot\omega\right)^2 + \left(k_1 + k_{12} + i\cdot\left(c_1 + c_{12}\right)\cdot\omega - m_1\omega^2\right)\cdot\left(k_2 + k_{12} + i\cdot\left(c_2 + c_{12}\right)\cdot\omega - m_2\omega^2\right)} \tag{A11}$$

A transfer function is a mathematical function that gives the system outputs for every possible value of the input; it provides information that specifies the behavior of the component in a system. In the case of MDOF system, the transfer function can be compacted into a transfer matrix $\underline{T}$ in which each component of the transfer matrix ($T(i,j)$) provides information about the response of the system at the DOF -i due to a unit force at the DOF -j. By analyzing the component $T(1,1)$ of the transfer matric $T(\omega)$ (i.e. the response of the DOF_1 due to a unit force at the DOF_1).

The steady-state vibration amplitudes for the 2DOF system by varying the mass (m_2), the stiffness of the DOF2 (k_2), and the stiffness of the connections (k_{12}) were investigated; the results in terms of T(1,1) are plotted in **Figure A 1**.

From the plots, when rigid connection is considered a) k_2/k_1 is significantly higher (k_2/k_1 higher than 8), or b) m_2/m_1 is significantly lower (m_2/m_1 lower than 1/10), the amplitude of the lowest resonance frequency is generally much greater than the highest frequency modes. For this reason, in this case, it is often sufficient to consider only the lowest frequency mode in the design calculations.

It is worth noting that, to apply this simplification when the connection is not rigid, the hypothesis of equal displacement of the 2DOF system becomes essential. Consequently, this simplification is considered acceptable only when rigid elastic connections are considered.

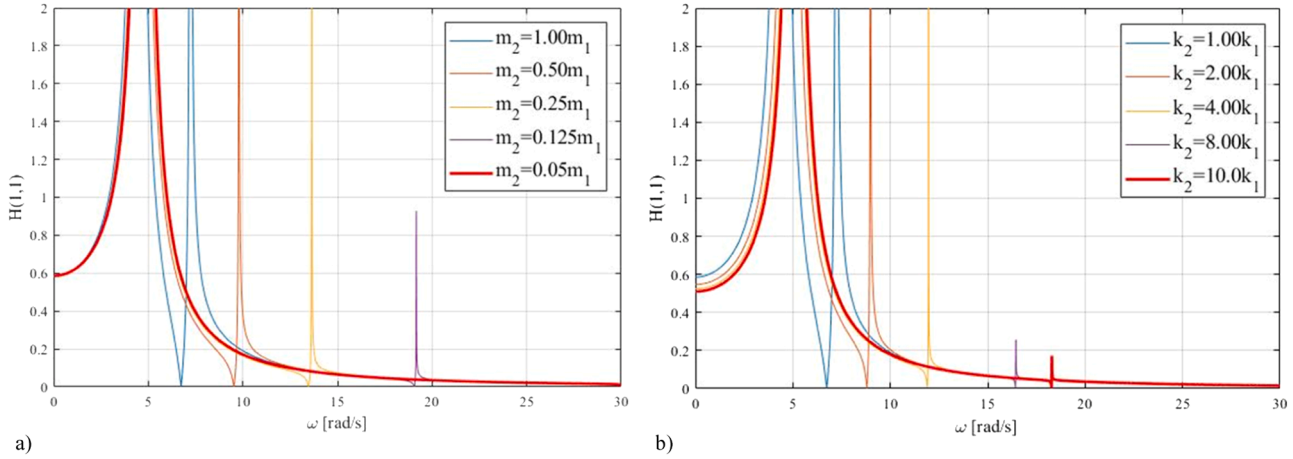

Fig. A 1. In-frequency response of the 2DOF system for a) m2 =m1, k2 = k1, for varying the retrofit stiffness k2; b) m2 =m1, for varying the retrofit stiffness k2; c) k2 = k1, for varying the mass (m2) of the retrofit system.

.

Appendix 2

See Tables A1 and A2 for geometry and steel rebars. Concrete C25/30 and steel Feb44k (design yielding stress equal to 430 MPa) were considered. Columns detailing. Note: Stirrups Φ6/150 mm.

Ground Floor (GF-F1)			
Column ID	*Lx (cm)*	*Ly (cm)*	*Longitudinal rebars*
P(1 to 9) and P(17 to 23)	30	30	4Φ16
P(10 to 16)	35	35	4Φ16
First Floor (F1-F2)			
Column ID	*Lx (cm)*	*Ly (cm)*	*Longitudinal rebars*
P(1 to 9) and P(17 to 23)	30	30	4Φ13
P(10 to 16)	30	30	4Φ16
Second Floor (F2-F3)			
Column ID	*Lx (cm)*	*Ly (cm)*	*Longitudinal rebars*
P(1 to 9) and P(17 to 23)	30	30	4Φ12
P(10 to 16)	30	30	4Φ13
Third Floor (F3-F4)			
Column ID	*Lx (cm)*	*Ly (cm)*	*Longitudinal rebars*
P(1 to 9) and P(17 to 23)	30	30	4Φ12
P(10 to 16)	30	30	4Φ12

Staircase walls. Note: Stirrups Φ6/250 mm.

All Floor (GF-F4)			
Wall ID	*Lx (cm)*	*Ly (cm)*	*Longitudinal rebars*
S1, S2	597	20	30Φ16 (in 2 rows)

Beams detailing. Note: same beam elements at each floor.

Longitudinal edge beam				Midspan section		Section at supports	
Beam connecting Columns	*Base (cm)*	*Height (cm)*	*Stirrup*	*Top rebars*	*Bottom rebars*	*Top rebars*	*Bottom rebars*
P(1 to 9) and P(17 to 23)	65	23	2Φ6/150 mm	3Φ16 + 3Φ11	2Φ12	3Φ16 + 3Φ11	2Φ12
Transversal edge beam				Midspan section		Section at supports	
Beam connecting Columns	*Base (cm)*	*Height (cm)*	*Stirrup*	*Top rebars*	*Bottom rebars*	*Top rebars*	*Bottom rebars*
P(1 to 17) and P(9 to 23)	30	50	2Φ6/150 mm	3Φ12	3Φ12	3Φ12	3Φ12
Central beam				Midspan section		Section at supports	
Beam connecting Columns	*Base (cm)*	*Height (cm)*	*Stirrup*	*Top rebars*	*Bottom rebars*	*Top rebars*	*Bottom rebars*
P(10 to 16)	100	23	4Φ6/150 mm	5Φ16 + 4Φ10	2Φ10 + 5Φ11	5Φ16 + 4Φ10	2Φ10 + 5Φ11

References

[1] Ambraseys NN, Smit P, Douglas J, Margaris B, Sigbjornsson R, Olafsson S, Costa G. Internet site for European strong-motion data. Boll di Geofis Teor Ed Appl 2004;45(3):113–29.

[2] Belleri A. Displacement based design for precast concrete frames with not-emulative connections. Eng Struct 2017;141:228–40.

[3] Belleri A, Marini A. Does seismic risk affect the environmental impact of existing buildings? Energy Build 2016;110:149–58. https://doi.org/10.1016/j.enbuild.2015.10.048.

[4] BPIE. Europe's Buildings Under the Microscope: A Country-by-Country Review of the Energy Performance of the Buildings. Brussel; 2011.

[5] Ciampi V, De Angelis M, Paolacci F. Design of yielding or friction-based dissipative bracings for seismic protection of buildings. Eng Struct 1995;17(5):381–91.

[6] D'Agostino D, Faiella D, Febbraro E, Mele E, Minichiello F, Trimarco J. Steel exoskeletons for integrated seismic/energy retrofit of existing buildings - general framework and case study. J Build Eng 2024;83:108413. https://doi.org/10.1016/j.jobe.2023.108413.

[7] Decanini, L., Gavarini, C., & Bertoldi, S. Telai tamponati soggetti ad azioni sismiche, un modello semplificato: confronto sperimentale e numerico. VI Convegno Nazionale di Ingegneria Sismica in Italia. Perugia; 1993.

[8] Di Lorenzo G, Colacurcio E, Di Filippo A, Formisano A, Massimilla A, Landolfo R. State-of-the-art on steel exoskeletons for seismic retrofit of existing RC buildings. Ing Sismica 2020;37(1):33–50.

[9] Di Lorenzo G, Tartaglia R, Prota A, Landolfo R. Design procedure for orthogonal steel exoskeleton structures for seismic strengthening. ISSN 0141-0296 Eng Struct 2023;275(Part A):115252. https://doi.org/10.1016/j.engstruct.2022.115252.

[10] EC8. (CEN). Design of structures for earthquake resistance. Brussels, Belgium: European Committee for Standardization; 2005.

[11] Faiella, D., Argenziano, M., Esposito, F., & Mele, E. Edifici Esistenti in Zona Sismica Adeguati Tramite Sistemi Strutturali in Acciaio (in italian). XXVIII CONGRESSO C.T.A. Francavilla al mare (CH); 2022.

[12] Faiella D, Faella V, Alaio E, Mele E. Adeguamento sismico di edifici esistenti in c.a. tramite esoscheletro diagrid. Costr Met 2019;5:9–23.

[13] Fajfar P. A nonlinear analysis method for performance-based seismic design. Earthq Spectra 2000;16(3):573–92.

[14] Feroldi, F. Sustainable renewal of the post WWII building stock through engineered double skin, allowing fro structural retrofit, energy efficiency upgrade, architectural restyling and urban regeneration. University of Brescia; 2014.

[15] Ferraioli M. Multi-mode pushover procedure for deformation demand estimates of steel moment-resisting frames. Int J Steel Struct 2017;17:653–76. https://doi.org/10.1007/s13296-017-6022-8.

[16] M. Ferraioli A. Lavino A. Mandara. An adaptive capacity spectrum method for estimating seismic response of steel moment-resisting frames; 2015. 33. 47–60.

[17] Gioiella L, Tubaldi E, Gara F, Dezi L, Dall'Asta A. Modal properties and seismic behaviour of buildings equipped with external dissipative pinned rocking braced frames. Eng Struct 2018;172:807–19. https://doi.org/10.1016/j.engstruct.2018.06.043.

[18] Guo JW, Christopoulos C. Performance spectra based method for the seismic design of structures equipped with passive supplemental damping systems. Earthq Eng Struct Dyn 2013:935–52. https://doi.org/10.1002/eqe.2261.

[19] Iervolino I, Galasso C, Cosenza E. REXEL: computer aided record selection for code-based seismic structural analysis. Bull Earthq Eng 2010;8:339–62.

[20] Kreslin M, Fajfar P. The extended N2 method taking into account higher mode effects in elevation. Earthq Eng Struct Dyn 2011;40(14):1571–89. https://doi.org/10.1002/eqe.1104.

[21] La Greca P, Margani G. Seismic and energy renovation measures for sustainable cities: a critical analysis of the Italian Scenario. Sustainability 2018;10(1):254. https://doi.org/10.3390/su10010254.

[22] Labò, S. Diagrid exoskeletons for the retrofit of RC Buildings. Holistic Sustainable Solutions to Renovate Post World War II RC Buildings in a Life-Cycle Perspective. (Supervisor: Alessandra Marini). (Vol. 19). Bergamo: University of Bergamo; 2021. doi:https://doi.org/10.6092/978–88-97413–45-5.

[23] Labò S, Passoni C, Marini A, Belleri A. Design of diagrid exoskeletons for the retrofit of existing RC buildings. Eng Struct 2020;220. https://doi.org/10.1016/j.engstruct.2020.110899. Retrieved from.

[24] Labò, S., Passoni, C., Marini, A., Belleri, A., & Riva, P. Design spectra for the preliminary design of elastic seismic retrofit solution from the outside. CreteIn: Proceedings of 7th International Conference on Computational Methods in Structural Dynamics and Earthquake Engineering (COMPDYN 2019); 2019.

[25] Labò, S., Passoni, C., Zanni, J., Milesi, M., Belleri, A., Marini, A., … Pelucco, S. Applicazione di interventi condotti dall'esterno ad un caso studio - edificio

residenziale in calcestruzzo armato". Report Reluis - WP5: Interventi di rapida esecuzione a basso impatto ed integrati. (in Italian); 2022 (available at: ⟨www.reluis.it⟩).
[26] Liu Y, Kuang JS. Spectrum-based pushover analysis for estimating seismic demand of tall buildings. Bull Earthq Eng 2017;15:4193–214. https://doi.org/10.1007/s10518-017-0132-8.
[27] Manfredi V, Santansiero G, Masi A, Ventura G. The High-Performance Dissipating Frame (HPDF) system for the seismic strengthening of RC existing buildings. Sustainability 2021;13(4). https://www.mdpi.com/2071-1050/13/4/1864.
[28] Marini A, Passoni C, Belleri A, Feroldi F, Preti M, Metelli G, Plizzari G. Combining seismic retrofit with energy refurbishment for the sustainable renovation of RC buildings: a proof of concept. Eur J Environ Civ Eng 2017:1–21. https://doi.org/10.1080/19648189.2017.1363665.
[29] Marini, A., Passoni, C., Riva, P., Negro, P., Elvira, R., & Taucer, F. Technology option for earthquake resistant, eco-efficient buildings in Europe: Research needs. Publications Office of the European Union; 2014. doi:10.2788/68902.
[30] Martelli L, Restuccia L, Ferro G. The exoskeleton technology as a solution to seismic adjustment of existing buildings. Procedia Struct Integr 2019;26:175–86. https://doi.org/10.1016/j.prostr.2020.06.021.
[31] Mazza F. Dissipative steel exoskeletons for the seismic control of reinforced concrete framed buildings. Struct Control Health Monit 2021;28(3):e2683. https://doi.org/10.1002/stc.2683.
[32] Mazza F, Donnici A. In-plane and out-of-plane seismic damage of masonry infills in existing r.c. structures: the case study of De Gasperi-Battaglia school in Norcia. Bull Earthq Eng 2021;19:345–76. https://doi.org/10.1007/s10518-020-00981-2.
[33] Mazza F, Donnici A. In-plane-out-of-plane single and mutual interaction of masonry infills in the nonlinear seismic analysis of RC framed structures. Eng Struct 2022;257:114076. https://doi.org/10.1016/j.engstruct.2022.114076.
[34] MidasGEN. Analysis Manual for Midas GEN; 2020.
[35] NTC. Norme Tecniche per le Costruzioni (NTC 2018). Gazzetta Ufficiale del 20/02/2018, Supplemento ordinario n.42; 2018.
[36] Passoni C, Guo J, Christopoulos C, Marini A, Riva P. Design of dissipative and elastic high-strength exoskeleton solutions for sustainable seismic upgrades of existing RC buildings. Eng Struct 2020;221. https://doi.org/10.1016/j.engstruct.2020.111057. Retrieved from.
[37] Passoni C, Marini A, Belleri A, Menna C. Redefining the concept of sustainable renovation of buildings: state of the art and an LCT-based design framework (January) Sustain Cities Soc 2021;64. https://doi.org/10.1016/j.scs.2020.102519.
[38] Porter, K. A Beginner's Guide to Fragility, Vulnerability, and Risk. University of Colorado Boulder; 2020, 128 pp., ⟨https://www.sparisk.com/pubs/Porter-beginners-guide.pdf⟩.
[39] Poursha M, Khoshnoudian F, Moghadam A. A consecutive modal pushover procedure for estimating the seismic demands of tall buildings. Eng Struct 2009;31(2):591–9. https://doi.org/10.1016/j.engstruct.2008.10.009.
[40] Rahmani A, Bourahla N, Bento R, Badaoui M. Adaptive upper-bound pushover analysis for high-rise moment steel frames. Structures 2019;20:912–23. https://doi.org/10.1016/j.istruc.2019.07.006.
[41] Reggio A, Restuccia L, Martelli L, Ferro GA. Seismic performance of exoskeleton structures. Eng Struct 2019;198. https://doi.org/10.1016/j.engstruct.2019.109459. Retrieved from.
[42] Sancin L, Bedon C, Amadio C. Novel design proposal for the seismic retrofit of existing buildings with hybrid steel exoskeletons and base sliding devices. Open Civ Eng J 2021;15:74–90. https://doi.org/10.2174/1874149502115010074.
[43] Santansiero G, Masi A, Manfredi V, Ventura G. Requalification of RC frame apartment buildings: comparison of seismic retrofit solutions based on a multi-criteria approach. Sustainability 2021, September 06. https://doi.org/10.3390/su13179962. Retrieved from.
[44] Sassun, K., Sullivan, T.J., Morandi, P., & Cardone, D. Characterising the in-plane seismic performance of infill masonry. Bulletin of the New Zealand Society for Earthquake Engineering; 2016.
[45] Smiroldo, F., Paviani, I., Giongo, I., Zanon, S., Albatici, R., Piazza, M.An Integrated Approach to Improve Seismic and Energetic Behaviour of RC Framed Buildings Using Timber Panels. Sustainability; 2021, 13(20). Retrieved from https://doi.org/10.3390/su132011304.
[46] Sucuoğlu H, Günay MS. Generalized force vectors for multi-mode pushover analysis. Earthq Eng Struct Dyn 2010;40(1):55–74. https://doi.org/10.1002/eqe.1020.
[47] The MathWorks, I. Matlab; 2017.
[48] Valluzzi, M.R., Masi, A. (Eds.). Low-Impact and Integrated Approaches for Seismic and Energy Retrofit of Built Heritage [Special Issue]. Sustainability; 2021.
[49] Verderame, G.M., Iervolino, I. & Manfredi, C.M.G. Il periodo nella valutazione sismica di edifici esistenti in c.a. Anidis 2007; 2007.
[50] Wen Y-K. Method for Random Vibration of Hysteretic System. J Eng Mech-asce 1976;102.
[51] Zanni, J., Cademartori, S., Marini, A., Belleri, A., Giuriani, E.P., Riva, P., … Luitprandi, G. Riqualificazione integrata e sostenibile di edifici esistenti con esoscheletri a guscio prefabbricati: il caso studio AdESA. Colloqui ATE. Nuovi orizzonti per l'architettura sostenibile. Catania; 2020.
[52] Zanni, J., Cademartori, S., Marini, A., Belleri, A., Passoni, C., Giuriani, E., … Marchetti, A.L.Integrated deep renovation of existing buildings with prefabricated shell exoskeleton. Sustainability; 2021, October 13. Retrieved from https://doi.org/10.3390/su132011287.
[53] Zanni, J., Labò, S., Passoni, C., Marini, A., Belleri, A., & Riva, P. Intervento di riqualificazione integrata strutturale energetica ed architettonica di edifici residenziali in ottica LCT (in italian). Francavilla al Mare (CH); 2022.